FATIGUE CRACK GROWTH CHARACTERISTICS OF OFFSHORE STRUCTURAL STEEL IN MARINE ENVIRONMENT

BIBHAS BHATTACHARYA

FATIGUE CRACK GROWTH CHARACTERISTICS OF OFFSHORE STRUCTURAL STEEL IN MARINE ENVIRONMENT

By

©BIBHAS BHATTACHARYA, B. Tech.

A Thesis submitted to the School of Graduate Studies in partial fulfillment of the requirements for the degree of Master of Engineering

Faculty of Engineering and Applied Science

Memorial University of Newfoundland

April, 1993

St. John's Newfoundland Canada

ISBN 0-315-86676-4

ABSTRACT

Corrosion fatigue of a metal is a more severe form of fatigue phenomena in the presence of a corrosive environment like seawater or sour gas. The enhanced fatigue crack growth rate has been attributed in part to the anodic dissolution (oxidation of metal) at the crack tip and to hydrogen embrittlement. Numerous studies have produced a wide variety of results regarding the effect of anodic dissolution and cathodic protection on the corrosion fatigue rate of high strength steel. Anodic dissolution can either cause an enhanced crack growth rate or a crack tip blunting causing a much delayed crack initiation or even a crack arrest. There is, however, some consensus about an optimum range of cathodic protection potential (-830mV SCE), around which the offshore steels achieve the maximum corrosion fatigue life. A more positive potential fails to stop the anodic dissolution. A more negative potential causes a higher crack growth rate, (most possibly by generation of hydrogen and hydrogen embrittlement). Micro-organisms, especially Sulfate Reducing Bacteria have been known to have enhanced metal corrosion fatigue. There are mainly two mechanisms responsible for such enhancement. During the respiration process hydrogen is consumed from the system which causes a cathodic depolarisation. Hydrogen sulphide is produced at the end of the respiration cycle, which is known for its contribution to hydrogen embrittlement.

It is important to understand more about the corrosion fatigue phenom-

ena of offshore structural steel in a marine environment. In the present study corrosion fatigue behavic of CSA G 40.21 M 350 WT steel is investigated. Tests were conducted in air, seawater and seawater with cathodic protection. Compact Tension specimens and ASTM substitute seawater had been used in the present study. Crack growth data was acquired using the Alternating Current Potential Drop technique. The data were then analysed according to the ASTM recommendation E647, 1981. A potential of -830 mV (SCE) was applied during the cathodic protection tests. The loading frequency was 3Hz in air and 0.167Hz in seawater. The air tests were conducted at room temperature and the seawater tests were conducted at 5°C. The stress ratio for all the tests was 0.05.

Multiple tests conducted in similar environments produced highly agreeable results. Free corrosion crack growth rate for the intermediate range of ΔK was about 1.5 to 2.0 higher than that in air. However, applying a cathodic protection of -830mV (SCE) reduced the crack growth rate to the level of crack growth rate in air. For all the corrosion fatigue tests (both cathodically protected and freely corroding) ΔK_{th} value was found to be higher than that in air.

ACKNOWLEDGEMENTS

The work for this thesis was carried out at the Faculty of Engineering and Applied Science, Memorial University of Newfoundland. Funding for the research was provided by Memorial University of Newfoundland. I am especially indebted to the Dean of the School of Graduate Studies, Dr. Malpas and the Associate Dean Dr. C. Sharpe for awarding me the fellowship.

I acknowledge the financial support provided by the Natural Sciences and Engineering Research Council of Canada through an operating research grant to Dr. K. Munaswamy, which made it possible to carry out the research.

I am grateful to Dr. K. Munaswamy who has acted as my supervisor and provided active help, advice and guidance throughout the course of the research. I must also thank Dr. R. M. Hopkins for his helpful inputs in the field of corrosion and corrosion fatigue. Added thanks to Dr. T. R. Patel from the Department of Biochemistry for acting as an advisor to the organic part of this project.

My thanks are also extended to the Technical Services for fabricating the experimental set up to its exacting requirements and to the technicians of the Structural Laboratory, especially Mr. Austin Bursey, for their constant help during the period of the study.

Contents

List of Figures

List of Tables

List of Symbols

SCE	Saturated Calomel Electrode.
ASTM	American Society for Testing of Materials.
ΔK_{th}	Threshold stress intensity factor.
ΔK_{max}	Maximum stress intensity factor.
ΔK_{min}	Minimum stress intensity factor.
ΔK_{Ic}	Critical stress intensity factor.
ΔK	Stress intensity factor.
a	Crack length.
N	Cycle count.
da/dN	Crack growth per unit cycle, crack growth rate.
SRB	Sulphate Reducing Bacteria.
ACPD	Alternating Current Potential Drop (technique).
P_{max}	Maximum load.
P_{min}	Minimum load.
ΔP	Load range, (P_{max}-P_{min}).
R	Stress ratio, (P_{max}/P_{min}).
ρ	Crack tip radius of curvature.
CT	Compact Tension (specimen).
V_1, V_2, V_3	Potential drop between probes at crack length a=0.
V'_1, V'_2, V'_3	Potential drop between probes at crack length a$\neq$0.
r	Distance between reference distance (reference distance).
c	Surface distance between active probes at crack length a $\neq$0.

Chapter 1

INTRODUCTION

1.1 Corrosion Fatigue of Offshore Structures

Due to a number of reasons corrosion fatigue plays a crucial role in the failure of the offshore structures. A typical offshore structure experiences a large number of (about 10^7) very low frequency (average 0.167 Hz) loading. This, in conjunction with a chemically active aqueous environment can pose a serious threat to any structural system. Offshore structures are usually made of high strength steels with good toughness characteristics but are very much prone to hydrogen embrittlement.

Factors affecting the corrosion fatigue resistance of a metal can be of metallurgical, mechanical or environmental origin. Among the mechanical variables which govern the crack growth rate are the loading frequency, wave form, stress ratio and the stress intensity range, ΔK . Environmental factors include environmental chemistry, pH, temperature, electrochemical potential and local organic activity (bio fouling).

It is known that bacteria (especially sulphate reducing bacteria) have a considerable ability to enhance corrosion fatigue in marine structures. Several models have been suggested to explain the microbial corrosion fatigue phenomena. According to the classical theory, the metabolic consumption of hydrogen by the bacteria causes depolarization (and enhanced corrosion) at the crack tip. Hydrogen sulfide on the other hand can poison the hydrogen recombination reaction resulting in a greater permeation of atomic hydrogen into the region of high triaxial stress, causing hydrogen embrittlement. However, the classical theory has come into severe attack mainly from researchers like King and Miller (1971). Role of biologically produced sulfide in enhanced corrosion rate has become important. Possibility of phosphate in causing major corrosion has also been investigated.

Given the background of the corrosion fatigue problem in offshore structures, a real need emerges to obtain more quantitative knowledge of the problem. This will give rise to a more efficient means to design the offshore structures as well as to protect them.

1.2 Scope and the objective

It is important to obtain the fatigue properties of offshore structural steels in a seawater environment. The results should be in a form directly applicable in the disign process. Also, the tests should conform to a widely accepted standard. This allows comparison of the test results and qualitative judge-

ment on the performance of the metal in question. In the current study the fatigue behaviour of an offshore structural steel, CSA G 40-21 grade 350WT, is investigated under corrosive environments. Particular attention is paid to the effects of seawater free corrosion and cathodic protection on the fatigue crack growth rate.

The fatigue tests are carried out in the following environments,

1. Air,

2. ASTM synthetic seawater (freely corroding) at 5°C,

3. ASTM seawater with -830mV(SCE) cathodic protection at 5°C.

The test setup was designed closely following the ASTM standard E-647 (1981). ASTM Compact Tension specimen was chosen as the test specimen. ASTM synthetic seawater (ASTM, Designation: D1141-75, 1990) was chosen as the main medium during the corrosion fatigue tests. At least two tests were conducted in each environmental conditions to check the repeatability of the results and confirm the effectiveness of the test setup. It is expected that the data published in terms of the plots of the stress intensity factor range (ΔK) and the crack growth rate (da/dN) would be a good source of fatigue design data for the CSA G 40-21, grade 350WT steel.

The present study is a precursor to another set of experiments investigating the effect of sulphate reducing bacteria on fatigue of steels. They include tests in 1) nutrient rich seawater and 2) seawater inoculated with bacteria.

Some work has been already done to that end and are reported in Appendix A.

Chapter 2

LITERATURE STUDY

2.1 Introduction

Corrosion fatigue occurs in metals as a result of the combined action of a cyclic stress and a corrosive environment. At the simplest level it can be attributed to the anodic dissolution of the metal mass at the crack tip. But in the real life it can be much more complicated than that. Accompanying the dissolution reaction at the crack tip are two possible cathodic reactions:

1. the reduction of dissolved oxygen to hydroxyl ions and

2. the reduction of hydrogen ions to atomic hydrogen.

Effect of the first reaction is protective in the form of metal hydroxide deposits on the metal surface. The second reaction, on the other hand, is the most damaging to the metal. The atomic hydrogen adsorbed into the metal surface may subsequently diffuse into the metal lattice at the zone of high tri-axial stress. The high equilibrium pressure of hydrogen inside the lattice affects

the integrity of the metal, making it susceptible to cracking at lower load conditions.

In summary, the localized dissolution (anodic reaction) at the crack tip may result in a higher fatigue crack growth rate or reduction in the same (Harty and Nöel, 1990) by means of crack tip blunting. On the other hand, the adsorption of hydrogen at the local cathodes may cause metal embrittlement ahead of the crack tip and hence a higher crack growth rate. These possible mechanisms are in competition with each other and the one with the greatest over all kinetics will be the rate determining one.

One of the main goals of research in corrosion fatigue is to develop the capability to predict (during the design phase), the maximum crack growth rate under a given metal-environment set up. Any good prediction requires an understanding of the mechanisms involved which again are functions of several parameters related to material properties, loading and environment.

The present study investigates the effect of seawater and cathodic protection on the fatigue behaviour of steel. While designing a fatigue experiment, one has to choose a few parameters for the experiment, like, temperature, loading frequency, the level of cathodic protection etc. They have to lie in an acceptable limit. Also, knowledge of how these parameters may affect the fatigue behaviour, is important. This allows predicton of the fatigue behaviour of the metal in a different environment. A lot of work has been done in the past two decades to understand the role of these parameters, some of which

are summerized in this chapter.

2.2 Fatigue crack propagation

When the crack growth rate (da/dN) is plotted against the stress intensity factor range ΔK in a log-log scale the curve shows a sigmoidal relationship (Fig. 2.1). In region 1, ΔK asymptotically approaches a thershold value ΔK_{th}, below which there is virtually no crack growth. Region 2 shows a linear steady state crack growth that can be expressed by many available relationships (Paris and Erdogan, 1963). Region 3 depicts rapid progress of the crack as K_{max} approaches the material fracture toughness, K_{IC}.

The nature of the crack growth rate curve changes in a corrosive environment. For low tempered steels there is an upward shift of the lower part of the region 2. This means a lower ΔK_{th} and lower slope under corrosion. This trend continues with lowering of the frequency.

High strength steels sensitive to stress corrosion cracking are affected by a corrosive environment only above a certain stress intensity range, ΔK_{ISCC}. The value of ΔK_{ISCC} goes down with decreasing frequency.

For some metal-environment system (eg. titanium alloys in chloride ions and structural steel in hydrogen gas), region 2 tends to be horizontal. Such a portion of the curve is called the plateau region. The width of the plateau increases with decreasing frequency. Such a plateau formation usually indicates

hydrogen embrittlement.

The following subsections briefly intorduces different parameters affecting a corrosion fatigue experiment.

2.2.1 Cyclic frequency

Normally, a lower frequency enhances fatigue crack growth rate. Panasyuk and Romaniv (1980) observed that low and medium strength steels are affected by seawater only at lower frequency range. The crack growth rate at 10Hz was almost the same as in air. The rate increases steadily as frequency drops to 1Hz, below which there is no further effect of frequency.

Ouchi[1] et. al. (1990) suggested that the high rise time associated with a low frequency loading causes the higher crack growth. The mechanism responsible is hydrogen embrittlement, which dominates over anodic dissolution at low frequency.

2.2.2 Cyclic wave form

Ouchi[1] et. al. (1990) compared the effect of different loading wave forms. It was observed that wave forms with high rise time will cause more damage. The hold time and the fall time had little effect on the crack growth rate. This observation seems to be supported by the findings of Panasyuk and Romaniv (1980). A sinusoidal wave form produced similar result as a symmetric triangular wave form. Positive sawtooth wave (rapid loading) and square wave made the material insensitive to corrosion fatigue. But, a negative sawtooth

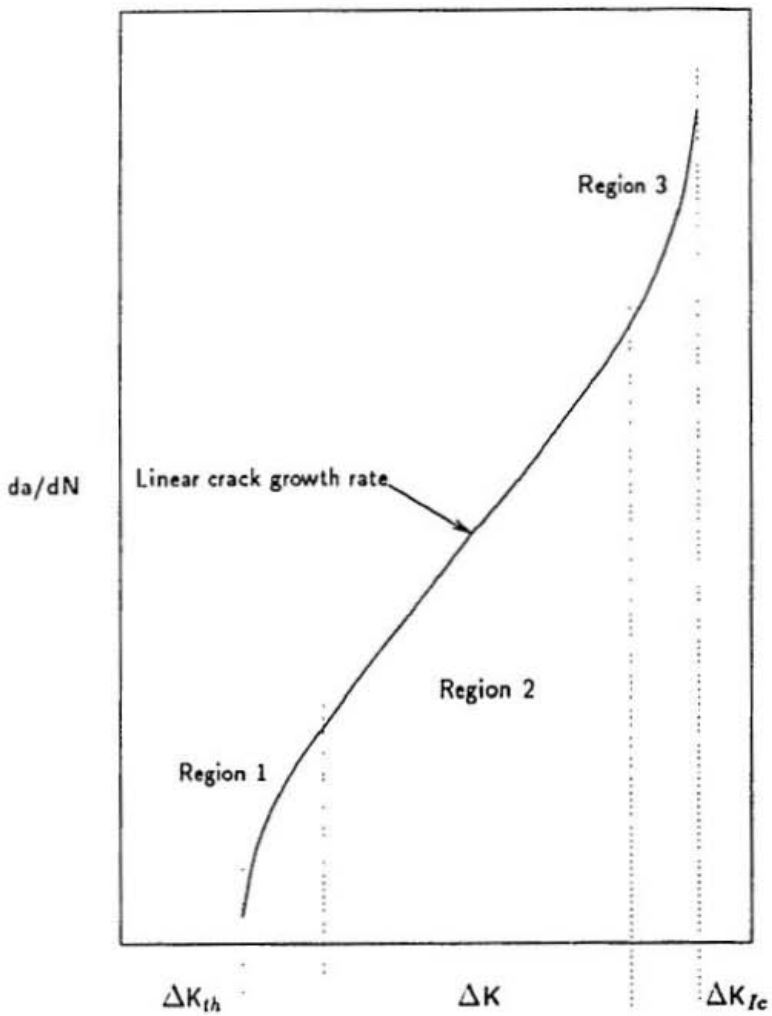

Figure 2.1: An ideal crack growth rate curve.

wave (rapid unloading) made the steel sensitive to corrosion.

2.2.3 Temperature

Ouchi[2] et. al., (1990), noticed that effect of water temperature(30° and 5°C) on free corrosion fatigue strength was extremely small. Venugopal and Putatunda (1990) observed that the crack incubation period decreases with temperature and the region II crack growth rate is enhanced by temperature.

2.2.4 Cathodic protection

The effect of cathodic protection on corrosion fatigue varies widely. Corrosion pitting and hence crack initiation could be delayed by cathodic protection. But it has been confirmed that a more negative cathodic potential increases the crack growth rate.

Maahn (1981) showed that the potential at the narrow crack level is different from the bulk environment. The reduction in potential inside the crack tip was mainly attributed to an ohmic drop caused by a hindered charge flow in and out of the crack tip. Consequently, this drop should depend on the crack opening and the width of the specimen. Brown (1983) presents a summary of studies on the effect of various cathodic protection levels on crack initiation and propagation of metals.

Jones and Blackie (1990) observed that, with a few exceptions, cathodic protection restores the corrosion fatigue life to the air level. The effect of decreasing the potential from -600mV to -1050mV varied from steel type to

steel type and from plain specimen to notched specimen. An optimum performance at -850mV was observed for most of the plain specimen and notched specimen. Though, on lowering the potential to -1050mV caused further improvement in fatigue life of a particular notched BS970 grade 817M40 steel.

Fuji and Smith (1983) observed that the aqueous environments generally causes a higher fatigue crack growth in HY-130 steel. The fatigue performance became close to that in air at very high ΔK values (of about 90MPa$\sqrt{m}$). Rajpathak and Hartt (1988) tested nine high strength steels for their corrosion fatigue crack initiation. A cathodic protection of -1.10 V (SCE) improved the fatigue performance. At higher frequency the specimen achieved the endurance limit. The free corrosion endurance limit was found to be less than that in air for all the steels.

Tubby and Booth (1992) tested single edged notched specimens made of high strength steels SAR 60 and MACS. SAR steel specimens tested in sea water without protection showed a crack growth rate 1.2 to 2.2 times the rate in air. A cathodic protection of -850mV at 5°C reduced growth rate below air. At 20°C the crack growth rates are found to be very close to the air values.

Rhee and Delgado (1992) tested high strength API 5AC C-90 riser coupling material compact tension specimens in air, seawater and brine environments. The crack growth rate in corrosive environment was significantly higher than that in air. The effect was more pronounced in the mid ΔK

region than for either a very low or high ΔK value. ΔK_{th} value increased with the duration of the tests, most probably because of higher deposition of calcareous materials. It is important to note that, a cathodic protection of -850mV(SCE) during the corrosion fatigue tests failed to bring down the crack growth rate to the air level.

Morgan et al. (1981) conducted corrosion fatigue experiments on structural steel. The stress ratio had no effect on fatigue crack growth rates in air but higher R ratio produced higher crack growth rates in seawater. Cathodic protection reduced the fatigue enhancement effect of sea water. A potential of -0.7V (Ag/AgCl) was found to be the optimum. More negative protection potentials resulted in an accelerated crack growth.

2.3 Sulfate reducing bacteria

Studies have related Sulfate reducing bacteria to enhanced corrosion and hydrogen embrittlement of metal. This section deals with their nutritional pattern and their possible role in microbial corrosion and hydrogen damage.

SRB's are basically non-phototrophic and acquire food from organic nutrients. They are also anaerobic and use sulphate as the electron acceptor. At the end of the respiration cycle sulphate is reduced to sulphide.

2.3.1 Nutrition

It is important to note (Hamilton, 1983) that SRB's have a very limited nutritional spectrum which is thermodynamic in origin. The span in redox potentials of the electron acceptor and electron donor gives a measure of the energy available to the organism from the respiration process. Considering hydrogen as the electron donor and sulphate as the acceptor SRB produces energy still far less than an aerobe. Consequently SRB's can only have an acceptor with redox potential less than -116mV to produce any energy.

It has been confirmed that molecular hydrogen acts as the electron donor. Oxidation of hydrogen occurs in the following manner:

$$SO_4^{2-} + 4H_2 \rightarrow S^{2-} + 4H_2O \tag{2.1}$$

The reaction is carried out by an enzyme called hydrogenase.

Figure 2.2 schematically shows the respiration process involved in the sulphate reducing bacteria.

2.3.2 Microbial corrosion

There are several proposed models trying to describe the mechanism of corrosion due to sulphate reducing bacteria. According to the classical theory which was proposed by Wolzogen Kuhr and Van der Vlugt in 1934, the SRB are responsible for a cathodic depolarisation caused by an uptake of hydrogen for their metabolism. The following series of reactions outline the classical

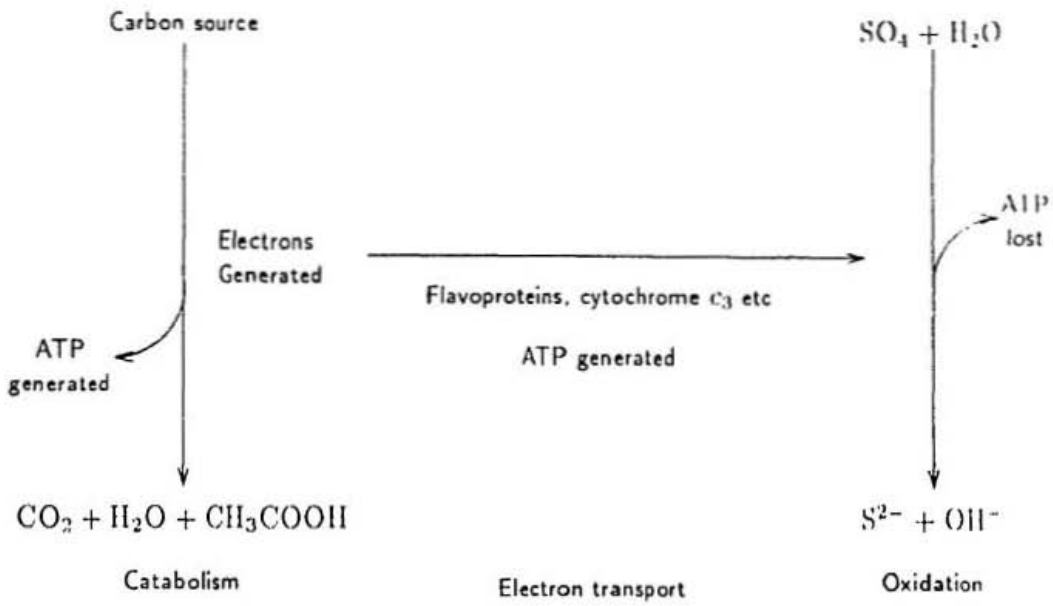

Figure 2.2: Respiration process in sulphate reducing bacteria

theory.

Anodic reaction:

$$8H_2O \rightarrow 8H^+ + 8OH^- \tag{2.2}$$

Cathodic reaction:

$$8H^+ + 8e \rightarrow 8H \tag{2.3}$$

Cathodic depolarization by SRB as in (eqn.2.1)

$$SO_4^{2-} + 8H^+ \rightarrow S^{2-} + 4H_2O \tag{2.4}$$

From this aspect the bacteria acts as an oxidizing agent increasing the corrosion current and making the steady state potential of steel more noble.

Corrosion product:

$$Fe^{2+} + S^{2-} \rightarrow FeS \tag{2.5}$$

Corrosion product:

$$3Fe^{2+} + 6OH^{-} \rightarrow 3Fe(OH)_2 \tag{2.6}$$

Over all reaction:

$$4Fe^{2+} + 4H_2O \rightarrow 3Fe(OH)_2 + FeS + 2OH^{-} \tag{2.7}$$

However the classical theory is not without it's deficiencies. The ratio of corroded iron to iron sulphide according to this theory (4:1) does not match with that found in actual cases (50:1).

A major challenge came from King and Miller (1971) in the wake of the observation that:

- there is no direct relationship between hydrogenase activity, the cause of depolarization according to the classical theory and the rate of corrosion.

- inorganically produced iron sulfide itself was found to depolarize cathodic steel in a bacteria free system.

This shifted the attention towards sulfide as the major cause of corrosion, though the basic set of reactions proposed by the classical theory remained unchanged.

A simulated corrosion experiment by Iverson (1966) failed to record the severity of a field corrosion test. In fact, a very little trace of reduced sulphate was noticed. Iverson and Olson (1983) tried to explain the event in a completely new light. Several phosphorous compounds (like, Fe_2P) were found as the universal corrosion products involving bacteria. It was suggested that, a highly reactive and volatile *phosphorus* compound which produces iron phosphide and phosphine among other things, is actually responsible for the corrosion.

Salvarezza and Videla (1980) conducted anodic polarization tests under the effect of SRB. The de-aerated salt solution curve had three distinct regions. The region between -660 mV to -600 mV showed a decrease in the current because of film passivation. Under aerated condition no such passivation was noticed. However in both the cases pitting potential was identical, about -580 mV. When the same specimen was tested in seawater contaminated with bacteria, an absence of any passivation and an overall reduction of pitting potential to about -700 mV was observed. The concentration of sulfide in the bulk solution had a noticeable effect on the anodic activity. Higher sulfide concentration increased anodic current and lowered pitting potential. The effect was even worse under a de-aerated condition. It was concluded that SRB enhances corrosion by removing passivation film and producing metabolic sulfide.

Daumas et al. (1988) studied corrosion induced by sulphate reducing

bacteria. A battery is constructed out of two half cells containing the same biological media (to support SRB life), one being sterile and the other being inoculated with bacteria. This allowed for testing the effect of both hydrogenase activity (oxidation of hydrogen) and H_2S. Another battery was made from a single cell. One of the electrodes was covered by a dyalisis membrane which allowed H_2S diffusion but protected the electrode from any hydrogenase activity. Cell potential and corrosion current was measured for all the cases. In the first battery, the cell carrying the inoculated medium achieved a higher (more noble) potential than the sterile cell. This indicated a cathodic depolarization caused either by sulfide or oxidizing agent hydrogenase. However, a very similar difference in potential was obtained in the second cell where both the electrodes were exposed to dissolved hydrogen sulfide and had equal deposition of iron sulfide on them.

Further study with the short circuit current between the two cells confirmed the domination of hydrogen oxidation as the dominant cause of corrosion. The effect of sulfide was eliminated since non sulfide producing bacteria gave rise to the same level of corrosion current.

2.3.3 Effect of H_2S on hydrogen permeation rate

H_2S, a bi-product of microbial metabolism, is often held responsible for an enhanced hydrogen embrittlement in metal. This subsection deals with the mechanism of H_2S related damage.

The enhanced stress corrosion cracking of steel in presence of hydrogen

sulfide, termed as sulfide cracking, is attributed to hydrogen embrittlement. Among the possible mechanisms, the poisoning effect of H_2S is the most popular one. According to this theory poisons like hydrogen sulfide increases the hydrogen overvoltage of iron. It has been suggested that the poisons get adsorbed to the surface of the metal and change the binding energy of adsorbed hydrogen to metal thus increasing the hydrogen overvoltage.

According to another theory hydrogen sulfide acts as a depolarizer rather than a polarizer and decreases the hydrogen overvoltage of iron. It gets adsorbed to the metal surface and enhances hydrogen adsorption by the following reaction.

$$H^+_{solution} + HS^-_{ads} \rightarrow (HSH) \xrightarrow{e^-} HS^-_{ads} + H_{ads} \qquad (2.8)$$

Turnbull and Carroll (1990) studied the effect of temperature and H_2S concentration on hydrogen diffusion and trapping in stainless steel in acidified salt sodium chloride solution. The results were analysed in terms of C_0, the concentration of hydrogen atoms below the surface of the metal exposed to hydrogen. This subsurface concentration was derived from the relation

$$J_\infty = DC_0/a \qquad (2.9)$$

Where, J_∞ is the steady state flux, D is the diffusion coefficient and a is the thickness of the medium. The diffusion coefficient was assumed to be the same as that for pure, annealed iron. The effect of trapping sites on the diffusion coefficient was neglected.

The C_0 value increased with higher H_2S concentration especially at higher temperatures.

Assefpour-Dezfuly and Ferguson (1988) studied the possible effect of hydrogen sulphide on fatigue crack growth. Hydrogen sulfide always gave rise to an increase in the crack growth rate and a plateau formation (indicative of hydrogen embrittlement). The combination of cathodic protection (-1.0 V) and hydrogen sulfide had the maximum deleterious effect.

Kawashima et. al. (1976) observed a higher susceptibility to hydrogen embrittlement in hydrogen sulphide solution. The effect was more pronounced for lower strain rate, lower pH and higher cathodic polarization.

2.3.4 Bacteria and hydrogen embrittlement

Sulphate Reducing Bacteria and marine fouling in general can increase the permeation of hydrogen in metals by locally altering the chemical environment and by producing agents like H_2S known to enhance hydrogen uptake of metals.

Cottis and Moore (1984) studied the hydrogen permeation current in presence of macro fouling. No major change in the rate was observed for each significant metabolic product introduced to the system. It was concluded that macro fouling does not bring about any damage by their own metabolism but helps create an anaerobic environment between the fouling mat and the metal surface. This in turn encourages the growth of sulphate reducing bacteria. It was recommended that sulphate reducing bacteria among the

fouling organisms should be treated as the main causative agent to increase hydrogen permeation in metal.

Cowling and Hancock (1985) studied the effect of sulphate reducing bacteria on fatigue on steel (BS 4360 Grade 50D). Crack growth rate in presence of bacteria was higher than in seawater added with nutrients. Further work was recommended to investigate the cause of the enhanced damage. Also, inorganically produced H_2S failed to simulate the severity of organically produced H_2S except at very low ΔK values.

Chapter 3

FATIGUE EXPERIMENTS

3.1 Introduction

The aim of the present research was to obtain fatigue crack growth characteristics of an offshore structural steel in the marine environment. The tests were to be conducted on standard ASTM compact tension specimens in air, ASTM seawater, with and without cathodic protection. It was expected that data from such a variety of environments could lead to a better understanding of the relative severity of seawater.

This chapter deals with the specimen, loading system, data acquisition system and environmental setup used in the current investigation. Table 3.1 summarizes the important parameters for all the tests. Figure 3.1 shows an over all view of the experimental set up.

Name	Max load (kN)	Load ratio	Frequency (Hz)	Environment	Protection (mV)(SCE)
A1	26.950	0.05	3	Air	-
A2	19.6	0.05	3	Air	-
A3	19.6	0.05	3	Air	-
S1	26.95	0.05	0.167	Seawater	-
S2	24.5	0.05	0.167	Seawater	-
S3	24.5	0.05	0.167	Seawater	-
C1	24.5	0.05	0.167	Seawater	-830
C2	24.5	0.05	0.167	Seawater	-830
N1	24.5	0.05	0.167	Nutrient	-830
N2	24.5	0.05	0.167	Nutrient	-830

Table 3.1: Experimental parameters

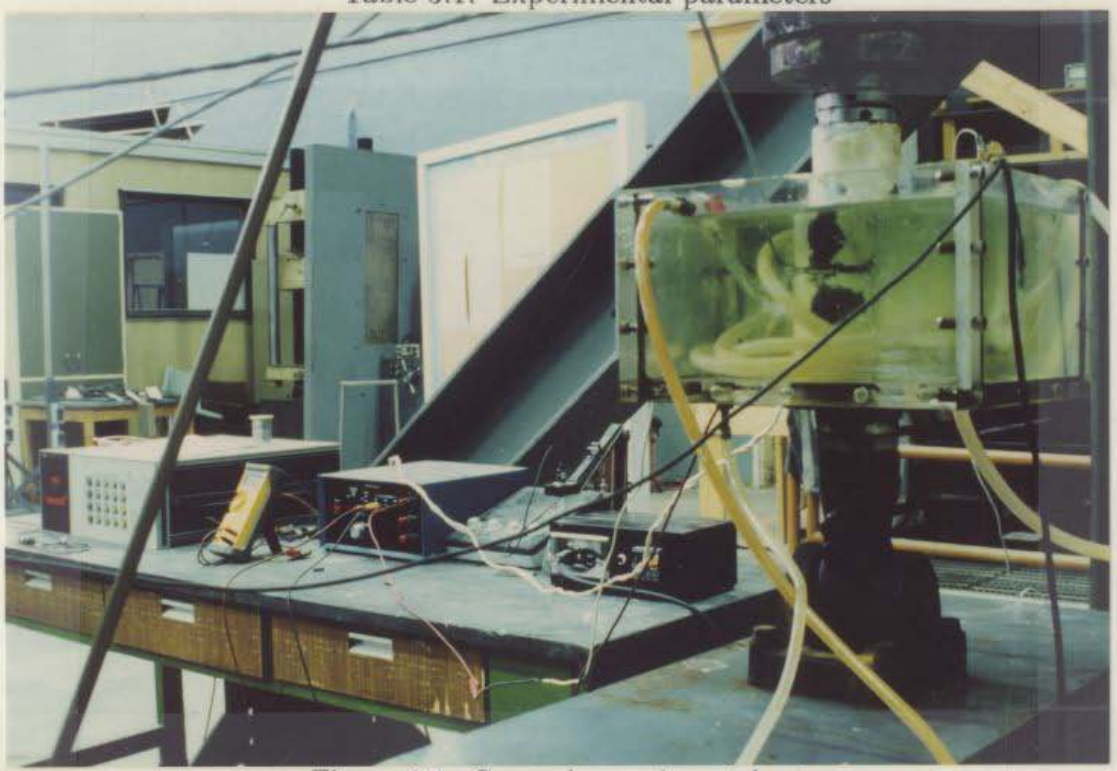

Figure 3.1: General experimental set up.

3.2 Specimen

The compact tension (CT) specimen is selected for the fatigue crack growth rate studies as ASTM E647-85 suggests the use of CT specimens whose planar dimensions can be chosen proportional to the thickness of the test specimen. More over larger height to width ratio provides an increased resistance to out of plane cracking and break off during high load testing.

The specimens were designed and fabricated such that fatigue crack surface is perpendicular to the rolling direction. The specimens were machined from 19mm thick steel plate which was manufactured to CSA G 40.21 M 350 WT specification. The dimensions of the specimen are shown in figure 3.2. The gripping fixtures used with these specimens are designed and fabricated in accordance with the requirements out lined in ASTM specification E647-85.

3.3 Instrumentation

3.3.1 Loading arrangement

Figure 3.3 shows the general loading arrangement. MTS hydraulics testing equipment (figure 3.4) was used to apply the fatigue load to the specimen. A vertical loading arrangement was chosen. The actuator was supported by an overhead I-Beam. At the end of the actuator a load cell and the top loading pin was attached. The bottom pin was supported by a strong

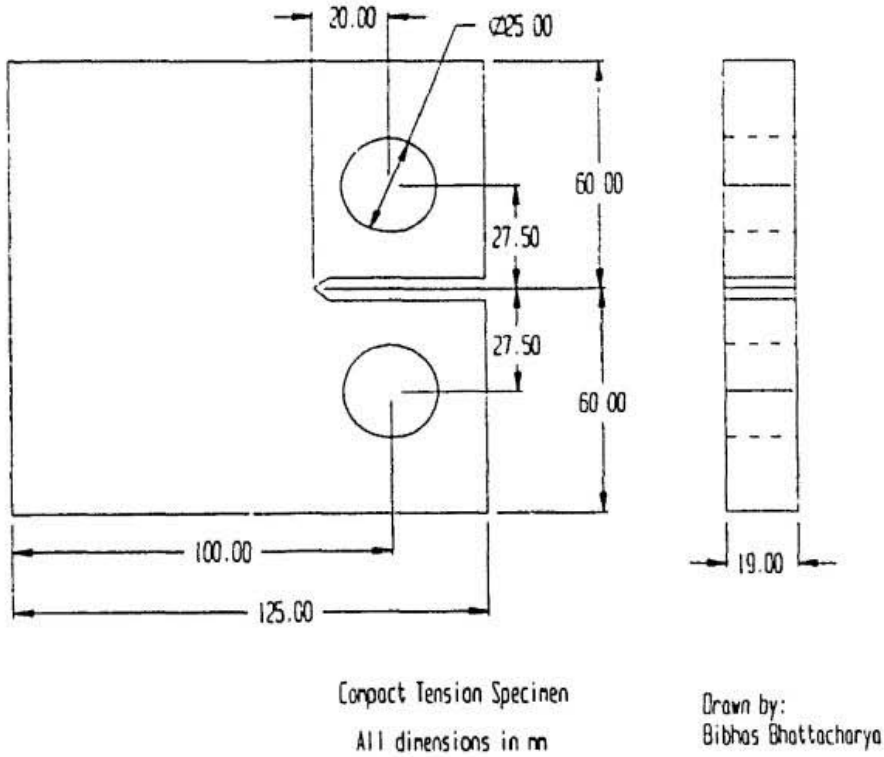

Figure 3.2: ASTM Compact Tension Specimen

platform which was designed to eliminate any kind of transverse motion. The set up is schematically presented in figure 3.3.

A PC based fatigue testing system MDT 1.1 was used to control the fatigue loading and for data acquisition (figure 3.5). Figure 3.6 schematically shows the load control system used. The signal from load cell goes to the MTS Controller where it is first amplified and demodulated by the Transducer Conditioner and then passed onto the Servo Controller by the Feedback Selector. The Servo Controller compares the feedback with a composite signal, the summation of the external program (MDT 1.1) and the set up of different parameters at the front control panel. If an error exists, an error signal is sent to the Servo Valve which opens in the direction and to

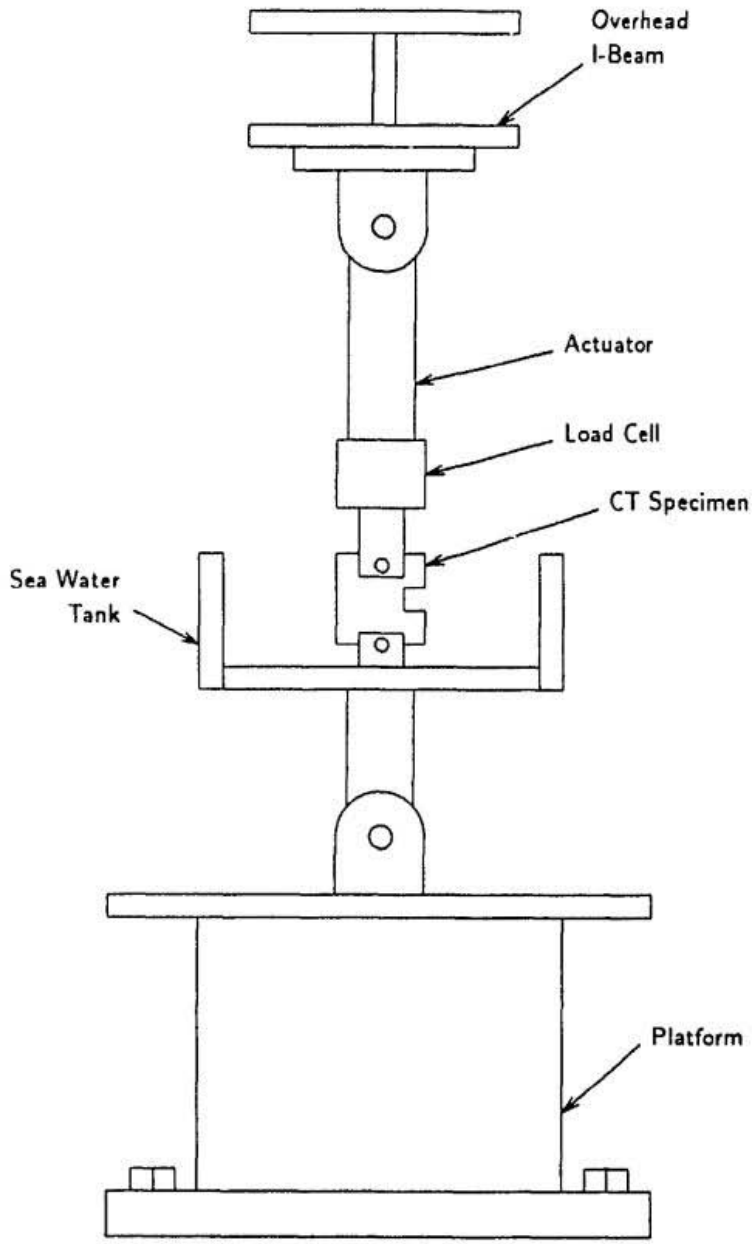

Figure 3.3: Loading arrangement.

Figure 3.4: MTS Hydraulic controller.

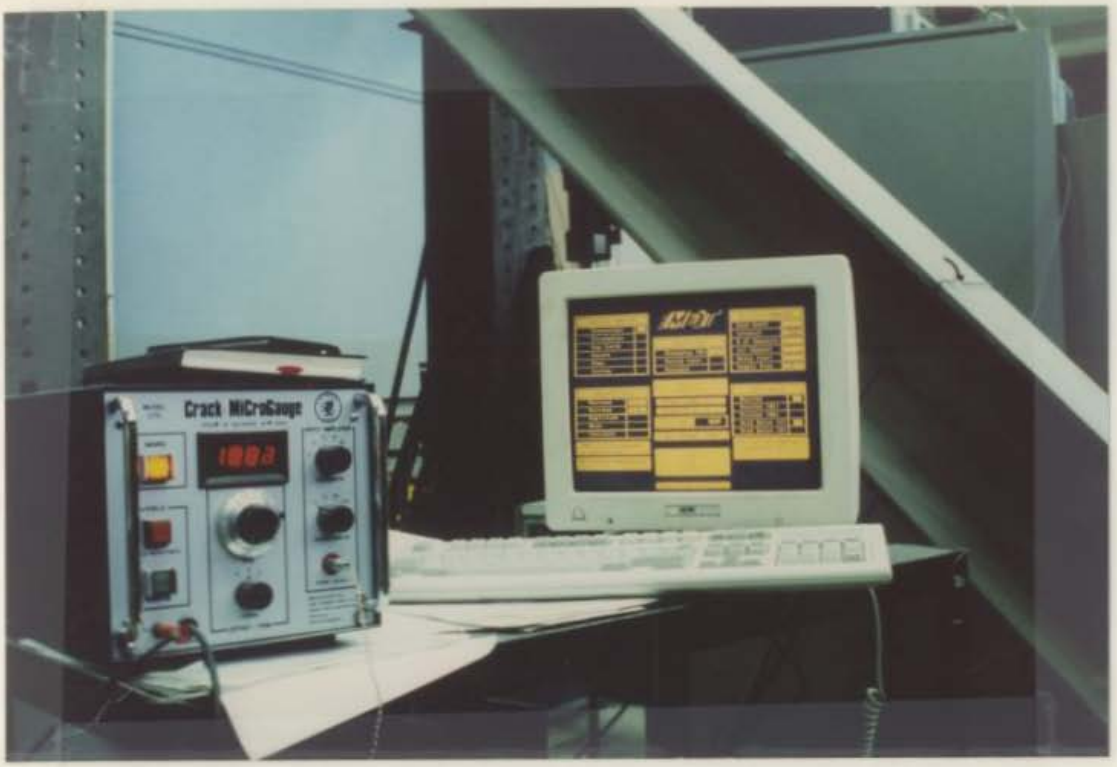

Figure 3.5: The Crack Micro Gauge and MDT testing software screen.

the extent necessary to correct the error.

3.3.2 Data acquisition procedure

Crack growth was monitored using an Alternating Current Potential Drop (ACPD) technique. The operation is simple. A high frequency AC field is applied to the specimen through two shielded field lead wires positioned at the front surface of the specimen (figure 3.7). Three probe wires are attached to the machined surface. Two of them are positioned across the notch tip forming the active probe pair. The other is placed on one of the machined surfaces which along with one of the active probes lying on the same surface forms the reference probe pair.

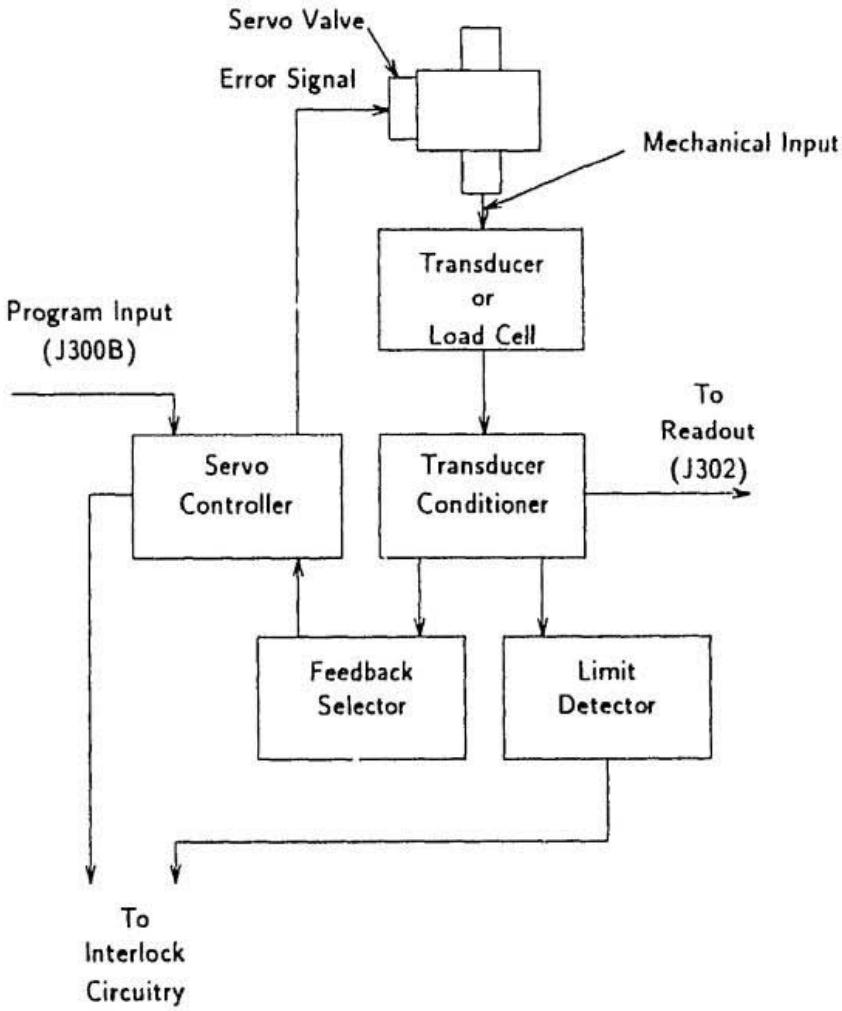

Figure 3.6: Load control flow chart.

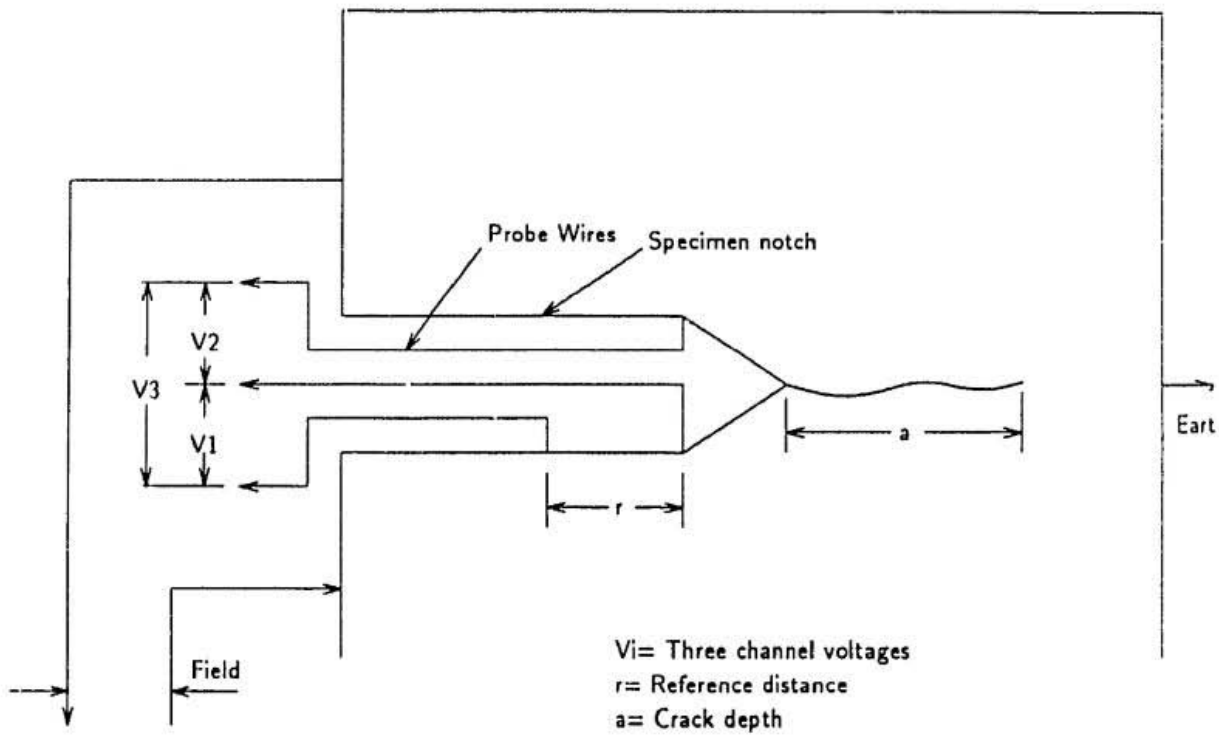

Figure 3.7: Three voltage channels used in ACPD measurements V_1= reference, V_2= crack and V_3= total voltages

Once the field is applied, a potential drop is created between the probes. This is because the surface length between them acts as resistance to the high frequency current. As shown in figure 3.7, V_1 represents the potential drop between the reference probes and V_2 represents the potential drop between the active probes. In absence of any crack the following relation holds,

$$r/V_1 = c/V_2 \tag{3.1}$$

Where, r is the reference distance and c is the net surface distance between the probes across the notch tip (active probes). As a crack initiates and increases in size, so does the surface distance between the active probes. This gives rise to an increased resistance and a higher potential drop (V_2) between the active probes. However, the reference voltage V_1 will have remained mostly unchanged. The relation in equation 3.1 now becomes,

$$r/V_1' = (2a + c)/V_2' \tag{3.2}$$

Where, V_1' and V_2' are the present potential difference between the reference and active probe pairs, respectively and a is the crack depth. Equations 3.1 and 3.2 give,

$$a = (c/2)(V_1'/V_2' - V_1/V_2) \tag{3.3}$$

Equation 3.3 was used to obtain the crack depth at any given point of time during the experiments.

3.3.3 Crack growth data acquisition

Figure 3.8 schematically represents the set up used to obtain crack growth rate data using the ACPD technique. The three probe wires are input to a Hewlett Packard scanner which switched between different pair of probe voltages (reference, crack and total, figure 3.7). The output of the scanner, is input to the crack micro-gauge for modulation. Then the voltages are recorded by the testing program.

Three sets of voltages, reference, crack and total, were read each time data was gathered. Upon the completion of a desired number of cycles the MDT program stopped the cyclic loading and held the specimen at a tensile load enough to prevent the crack surfaces from touching each other. Then it sent a signal to the scanner to close one of the three channels and read in the voltage. The voltage was input to the Crack Micro gauge which converted it into an amplified DC voltage which was then input into the PC to be stored in a data file. When all the three channels were read in, the cyclic loading resumed.

The impressed current from the Crack Micro Gauge was passed through a polarity reversing switch (before being applied to the specimen). This gave a chance to balance the Micro Gauge by comparing a channel voltage under both the polarities.

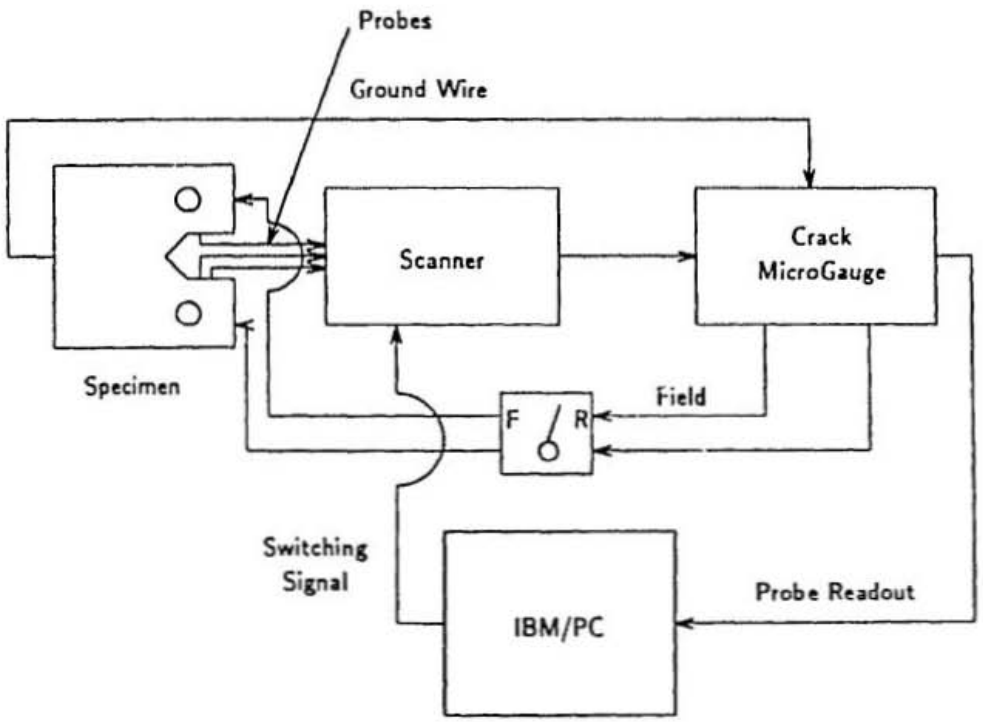

Figure 3.8: Schematics of the data acquisition system used.

3.4 Environmental setup

All the air tests were conducted under normal laboratory conditions at a frequency of 3Hz and stress ratio 0.05. Special environments were created for corrosion fatigue tests. Artificial seawater used in the experiment was prepared according to the ASTM Designation D1141-75. A plexiglass chamber (figure 3.9, 3.10 and 3.11) was used to hold the seawater and the specimen. The bulk of the seawater was kept in a bigger reservoir and slowly circulated through the test chamber. The water was cooled inside the reservoir by a refrigeration coil system which was completely covered by plastic tubing to prevent any corrosion of the actual copper coil. A temperature probe, inserted inside the test chamber provided the feedback to the refrigeration system ensuring a steady test temperature of 5°C. The seawater solution was kept at a pH level of around 8.2, as per the ASTM standards.

During the cathodic protection tests, the specimen was held at a potential of -830 mV with respect to a saturated calomel electrode (SCE). A potentiometer was used to polarize the specimen.

3.5 Experimental Procedure

3.5.1 Specimen preparation

The specimen is prepared for the test according to the nature of the test involved. During the corrosion fatigue tests specimens were painted with

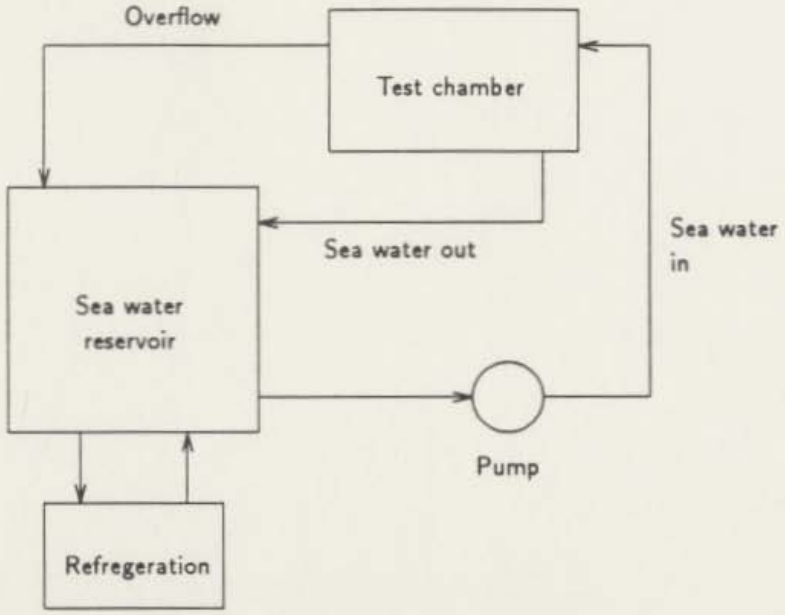

Figure 3.9: Seawater test setup

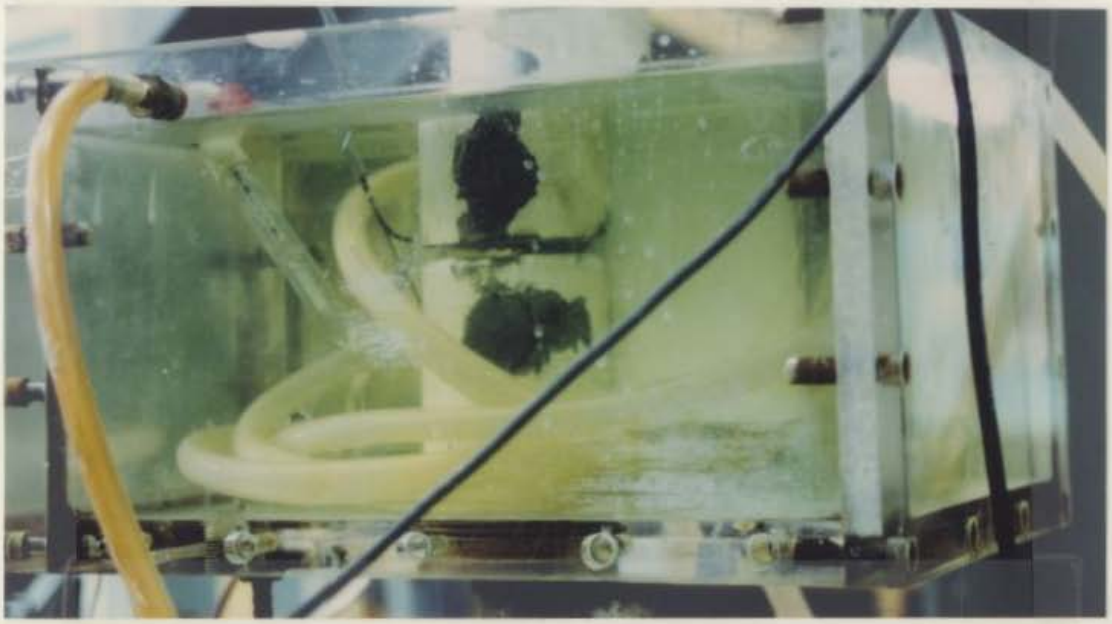

Figure 3.10: Side view of corrosion fatigue test chamber.

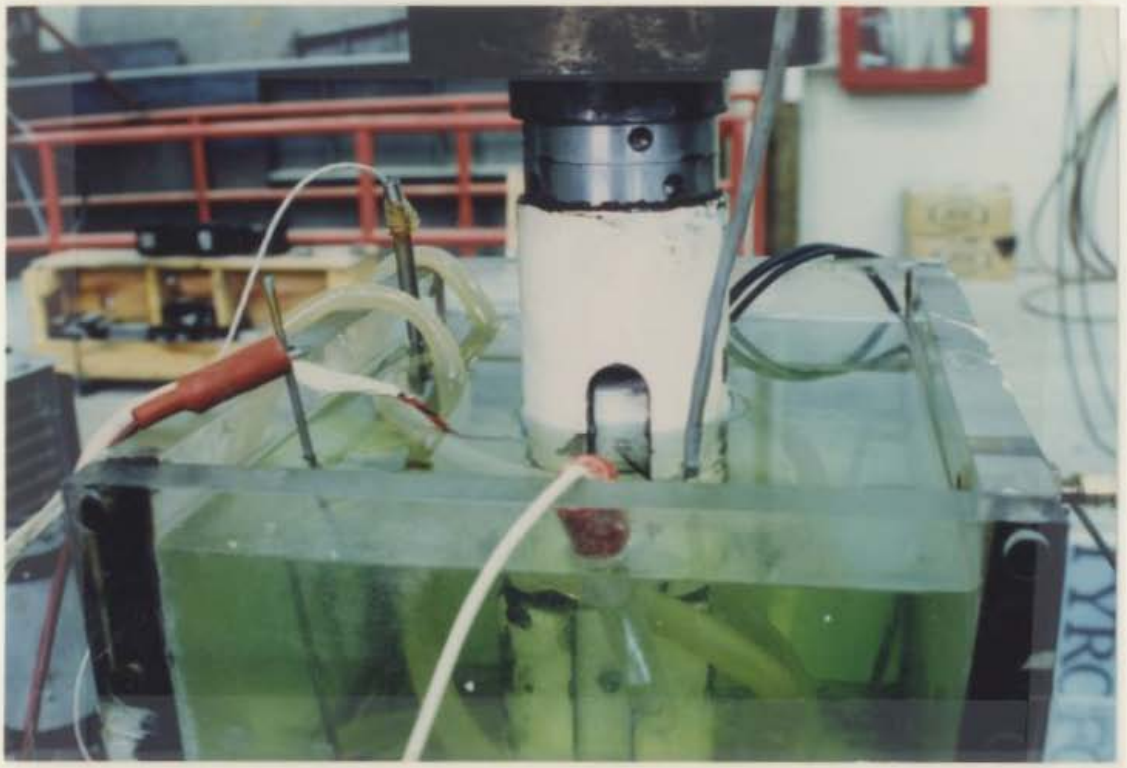

Figure 3.11: Top view of corrosion fatigue test chamber.

spray paint. The surface where crack profile is expected to grow is stripped of any paint. The notch tip of all the specimens were cleaned so that no metal scrap formed during the machining can plug the crack.

Three ACPD probes are spot welded to the specimen on the appropriate notch surfaces (Figure 3.7). Three thick copper wire stubs were spot welded, two to the front of the specimen and one to the back. Later the field wires were soldered to the copper wires on the front and the ground wire was soldered to the copper wire on the back.

Once all the necessary wires were fitted to the specimen the reference distance (r) was measured using a travelling microscope. Then the specimen was positioned in the testing rig.

3.5.2 Pre-cracking

The compact tension specimens were designed to produce crack growth rate data for a crack tip stress intensity range levels between 15 to 50 MPa$\sqrt{m}$. To conform to the ASTM standards all specimens were pre-cracked to 6mm (from notch tip) at room temperature using a constant amplitude sinusoidal load at a frequency of 6Hz. The precrack end-load was kept at 20% lower than the actual test load level. This eliminated any possibility of transient crack growth during the initial phase of the actual test.

For the seawater tests the specimens were pre cracked in air up to 4mm at a high frequency of 6Hz. The rest of the pre-cracking was done in the actual test environment at the actual test frequency of 0.167Hz.

3.5.3 Main test

The actual test load was chosen depending on the crack growth rate in the environment involved, so that enough number of data points could be obtained. It was attempted not to have the crack depth data points too close (less than 0.2 mm) or too far away (more than 1mm). Fatigue loading was continued until the specimen failed (during the air tests) or the crack reached close to the failure limit (during the corrosion fatigue tests). The later was to prevent any accidental breakage of the test chamber and spilling of seawater solution.

The following parameters were monitored from time to time to maintain

the test standards:

- The load waveform, for load value, frequency and waveform shape,
- Crack micro-gauge balance,
- Cathodic protection voltage,
- Temperature and
- pH of the solution.

Chapter 4

RESULTS AND DATA INTERPRETATION

4.1 Data acqusition

The fatigue testing program MDT1.1 maintained separate data files for each reading of the three ACPD probe voltages and the corresponding cycle number. A program, written for the purpose, gathered the data and calculated the crack depth using the equation 3.3. Then, as recommended by the ASTM standards, the seven point sliding method was applied to the data set to derive the ΔK vs da/dN values. The derived data was plotted and experimental error points, if any, are excluded. Once the data are finalized, the best fit lines are passed through them to evaluate the material constants.

4.2 Computation of crack growth rate and stress intensity factor range

Two separate computational procedures are involved to obtain the two parameters necessary to express a fatigue test result in a useful and geometry independent manner. One of these procedures calculates the stress intensity factor range, ΔK, from the discrete crack length measurements and the loading variables for the test specimen. The other involves computing the instantaneous fatigue crack growth rate $(da/dN)_i$, from the discrete measurements of the crack length (a_i) and the elapsed number of cycles (N_i). One only needs the raw crack length vs. number of cycles data to carry out the above to computations.

4.2.1 Stress intensity factor range evaluation

The variation in the stress intensity factor, ΔK, is defined using only the positive portion of the load cycle because of the assumption that ΔK is equal to zero when the crack faces are closed (close to the start of compressive load). For the compact tension specimen, ΔK is calculated using the following relation (ASTM E647-78T, 1981),

$$(\Delta K)_i = \frac{\Delta P}{BW}\frac{(2+\alpha)}{(1-\alpha)^{3/2}} \times \left[0.886 + 4.64\alpha - 13.32\alpha^2 + 14.72\alpha^3 - 5.60\alpha^4\right] \quad (4.1)$$

Where,

$$\begin{aligned} \Delta P &= P_{max} - P_{min}, \text{ Load range,} \\ B &= \text{Specimen thickness, see figure 3.2} \\ W &= \text{Specimen width,} \\ \alpha &= a/W, \\ a &= \text{Crack depth.} \end{aligned} \tag{4.2}$$

4.2.2 Crack growth rate evaluation

The instantaneous crack growth rate $(da/dN)_i$ is really the slope of the crack length (a) vs. elapsed cycle (N) curve at a given cycle N_i. A numerical technique can be applied to obtain the slope instead of actually recording it during the experiment. The present study uses the seven point curve fit method to obtain the crack growth rate.

4.3 Calibration

Six specimens were tested in air to calibrate the ACPD crack growth measurement setup. During these tests crack depth was measured both visually and by ACPD technique. For the visual measurement, beach marks were introduced on the fracture surface at frequent intervals. This was accomplished by fatigue loading the specimen at twice the main test frequency. To ensure a sharp beach mark, load range was reduced to half the main test

value. After the test was completed the specimen was broken apart and the crack lengths marked by the beach marks were measured using a travelling microscope.

Crack length values obtained using both the methods are plotted in figure 4.1. The best fit line drawn through all the data points yielded the following relation,

$$TM = 0.999263 \times ACPD + 0.370423 \tag{4.3}$$

Where, TM and ACPD are the crack depth measured by the travelling microscope and ACPD technique respectively. In light of the above discussion the ACPD crack depth values were deemed to be accurate enough and need for any correction was found unnecessary.

4.4 Results

The fatigue crack growth data (a vs N) for all the tests are shown in figure 4.2 through 4.9.

The crack growth rate data are presented graphically as log-log plots of crack growth rate (da/dN) and stress intensity factor range ΔK in figure 4.10 through 4.19. Individual tests are presented in scatter plots. Then the data from tests carried out at a particular environment are grouped together in one single plot. This gave a chance to evaluate the validity of the test results. As a next step, least square regression curve was fitted through a group of

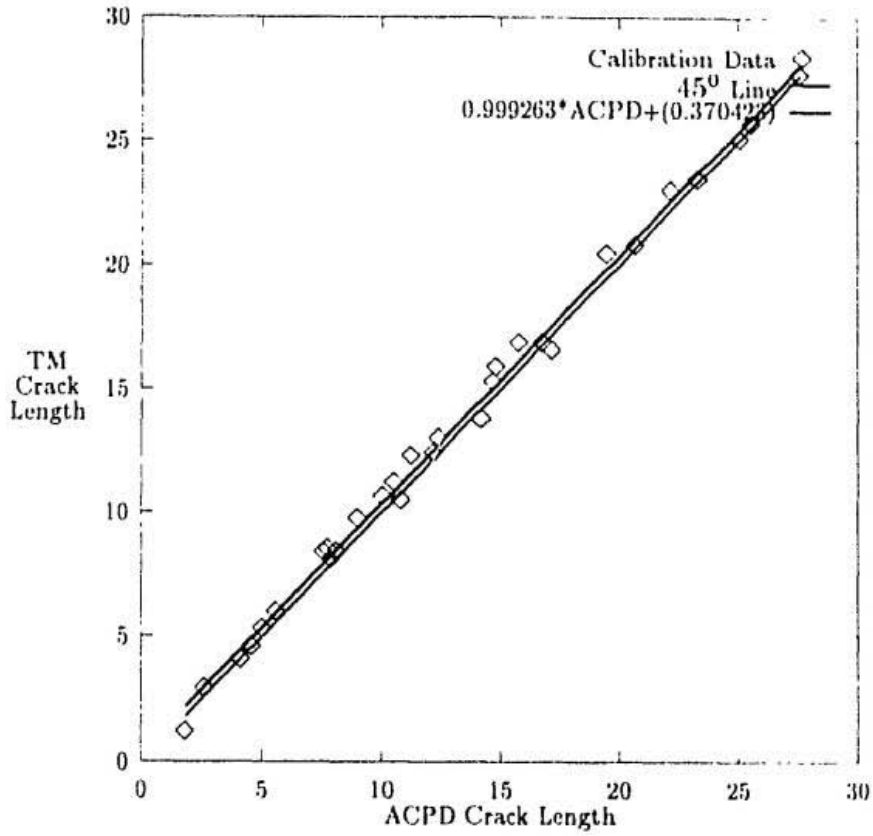

Figure 4.1: ACPD vs. TM crack depth.

data. The form of the equation in Paris' law (1963) was used in the least square program,

$$\frac{da}{dN} = C(\Delta K)^m \tag{4.4}$$

Where, C and m are called the material constants.

Due to the nonlinearity of the data points (in log-log scale) for the corrosion fatigue tests, more than one such curves were fitted to closely approximate the da/dN vs. ΔK plot. Table 4.1 lists the material constants derived from the best fit curves and the corresponding range of ΔK values.

ΔK Range	C	M
Air		
16.233 to 47.731	2.264259e-12	3.322270
Seawater		
20.126 to 27.003	4.202039e-13	4.003989
27.003 to 35.776	1.841166e-10	2.152813
35.776 to 48.475	3.143066e-08	0.713390
48.475 to 61.137	1.720893e-10	2.062689
Cathodic Protection		
20.939 to 21.841	1.810432e-23	11.819560
21.841 to 25.114	3.510724e-06	-1.138005
25.114 to 37.532	8.737302e-13	3.595440

Table 4.1: Material Constants

4.4.1 Air tests

Figure 4.10, 4.11 and 4.12 show the crack growth rate data for the three out of the five tests conducted in air. Finally they are combined in one plot (figure 4.13) and a single best fit line is passed through them.

The first specimen (A1) was tested at a higher load range. In order to obtain more number of data points it was decided to lower the load range and delay the failure of the specimen. However, from the combined plot it can be seen that load range had little effect on the crack growth rate. For the third specimen A3, there is a considerable scatter in the data below a stress intensity range of 16 MPa$\sqrt{m}$. The combined plot (figure 4.13) shows a very good agreement between the three test results showing the good repeatability of the experiment.

4.4.2 Free corrosion tests

The data for the seawater free corrosion tests are presented in figure 4.14, 4.15, 4.16 and finally in a combined plot figure 4.17. The first specimen (S1) was tested at a higher range (ΔP=25.628 kN) compared to the other two (ΔP = 23.298 kN). As seen in figure 4.14, specimen 1 crack growth rate showed a plateau behaviour below a ΔK value of 33MPa$\sqrt{m}$. Beyond that the crack growth behavior was identical to the other two specimens. In the superimposed plot (figure 4.17) four best fit lines were drawn to best represent the data set. During the best fit process only the portion of the

specimen 1 data that is similar to the other two is considered.

4.4.3 Cathodic protection tests

Figure 4.18 and 4.19 display the data for the two specimens tested in seawater with cathodic protection (-830 mV SCE). For most part the crack growth rate was indentical to the air values. Below a ΔK value of 25MPa$\sqrt{m}$ both the specimens showed a brief period of crack growth rate higher than in air. For first specimen C1, there is a sharp decrease in crack growth rate after ΔK = 26MPa$\sqrt{m}$. This corresponds to a loading system failure and shut down of the test for 6-7 hours. However, the crack growth rate again recovered to that of the specimen C2 near a ΔK value of 30MPa$\sqrt{m}$. Figure 4.20 shows the combined plot of the cathodic protection tests.

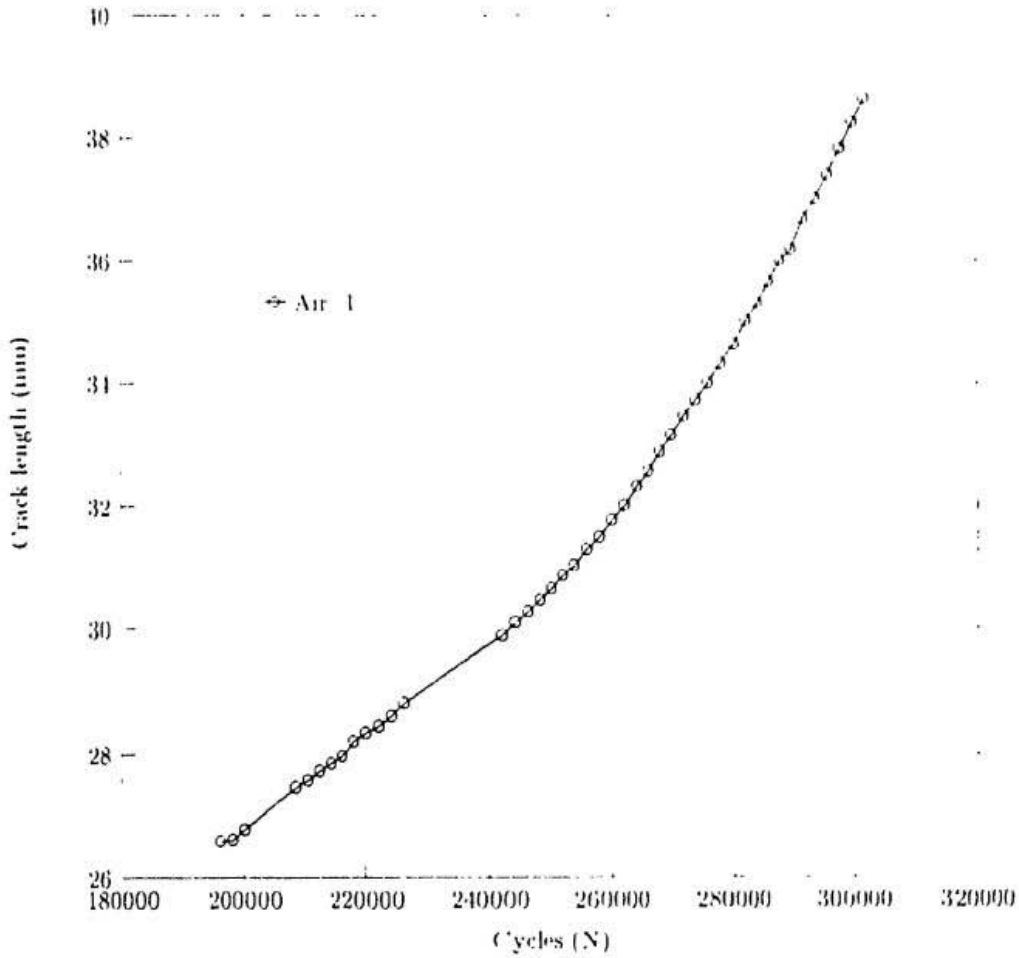

Figure 4.2: Crack growth curve for: air 1

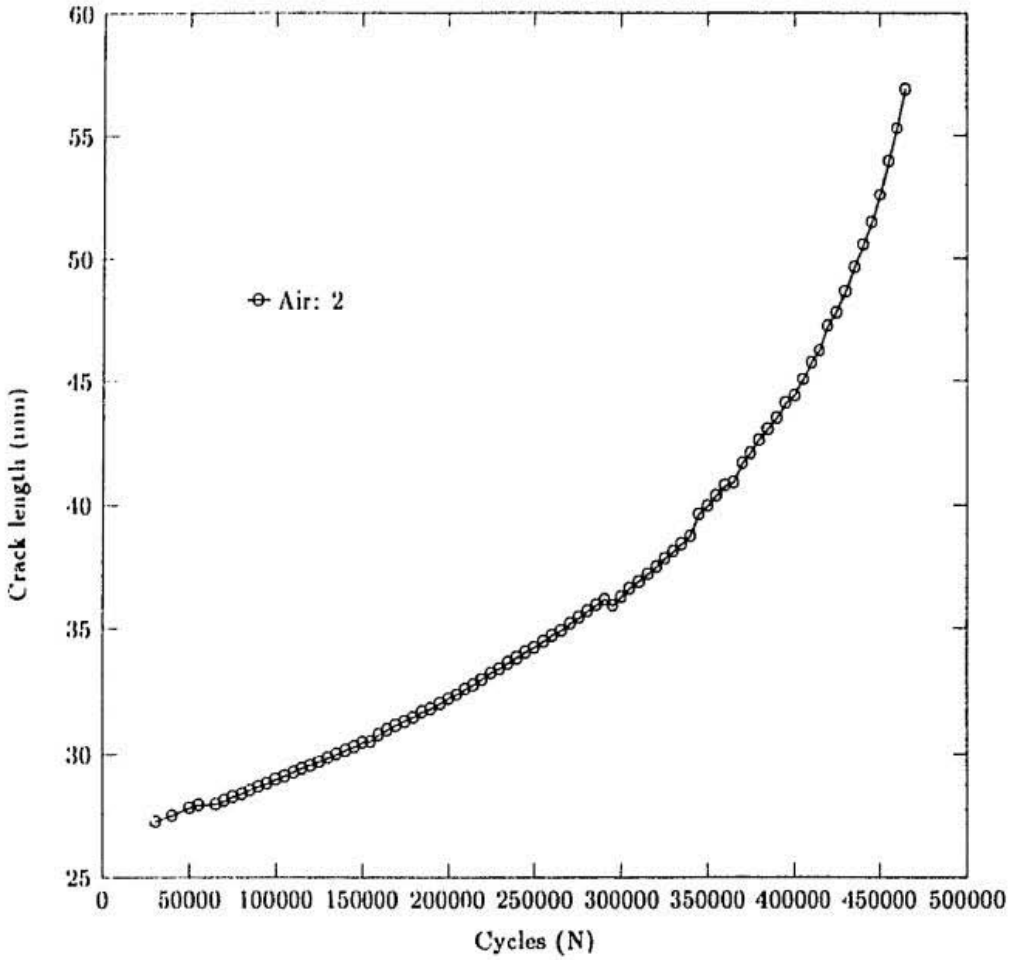

Figure 4.3: Crack growth curve for: air 2

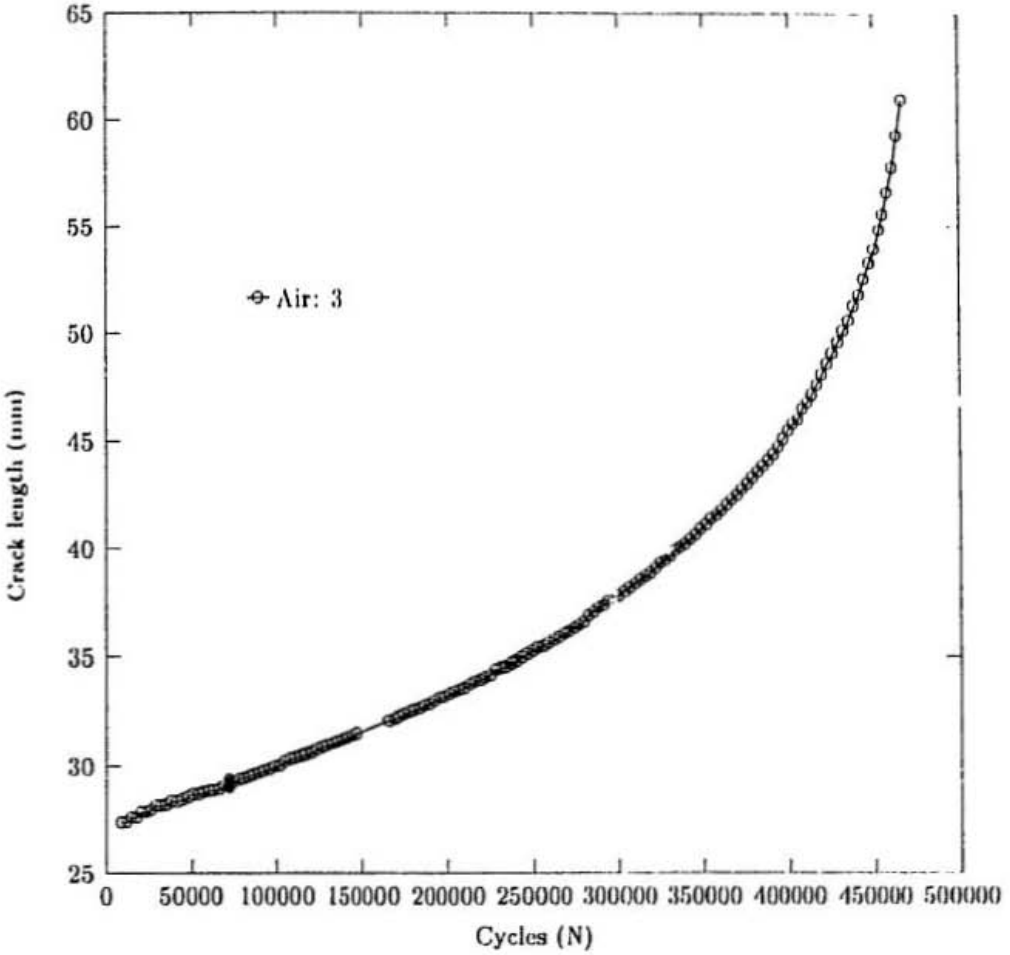

Figure 4.4: Crack growth curve for: air 3

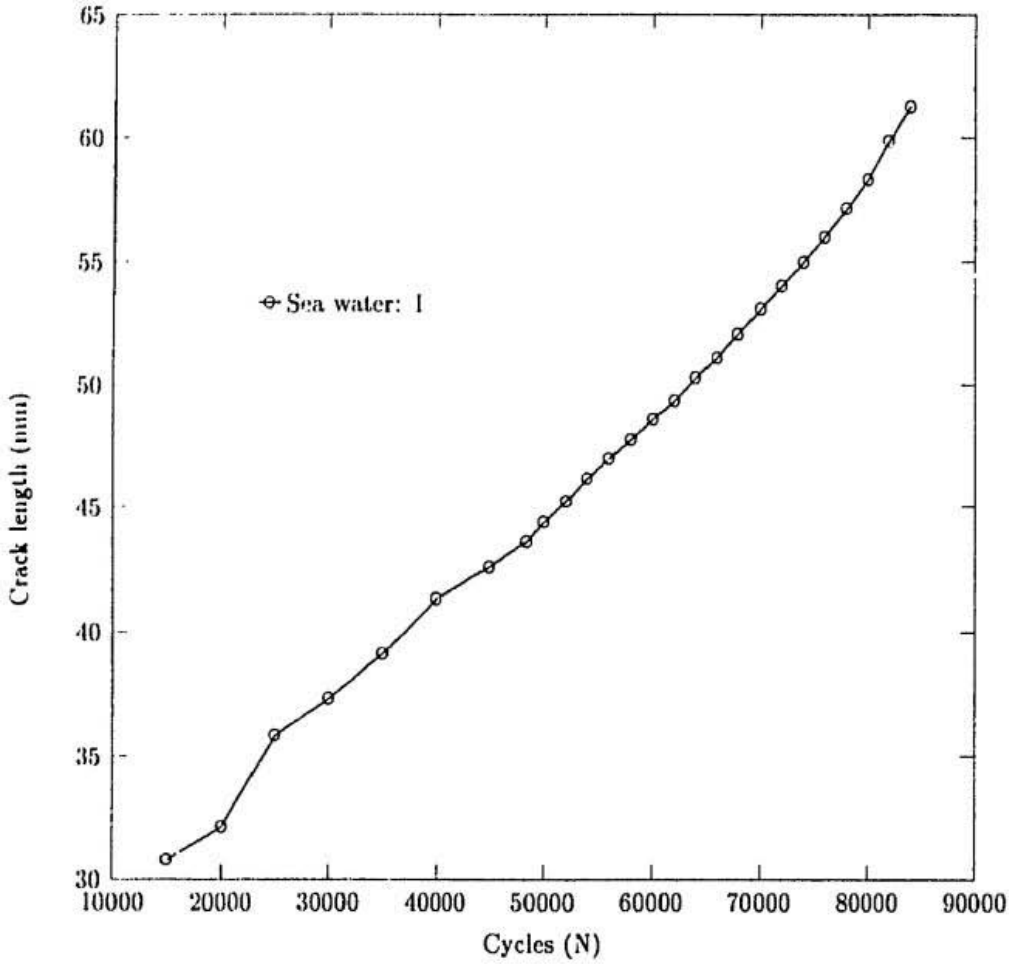

Figure 4.5: Crack growth curve for: sea water 1.

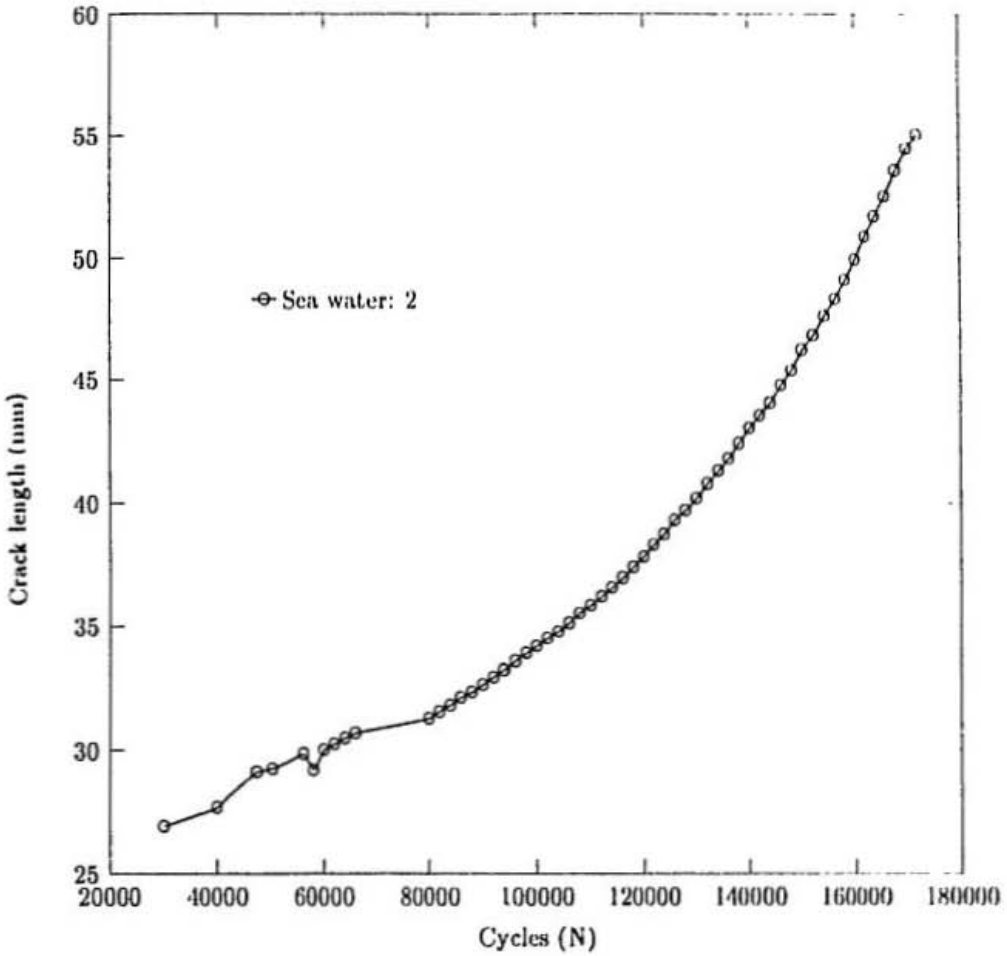

Figure 4.6: Crack growth curve for: sea water 2.

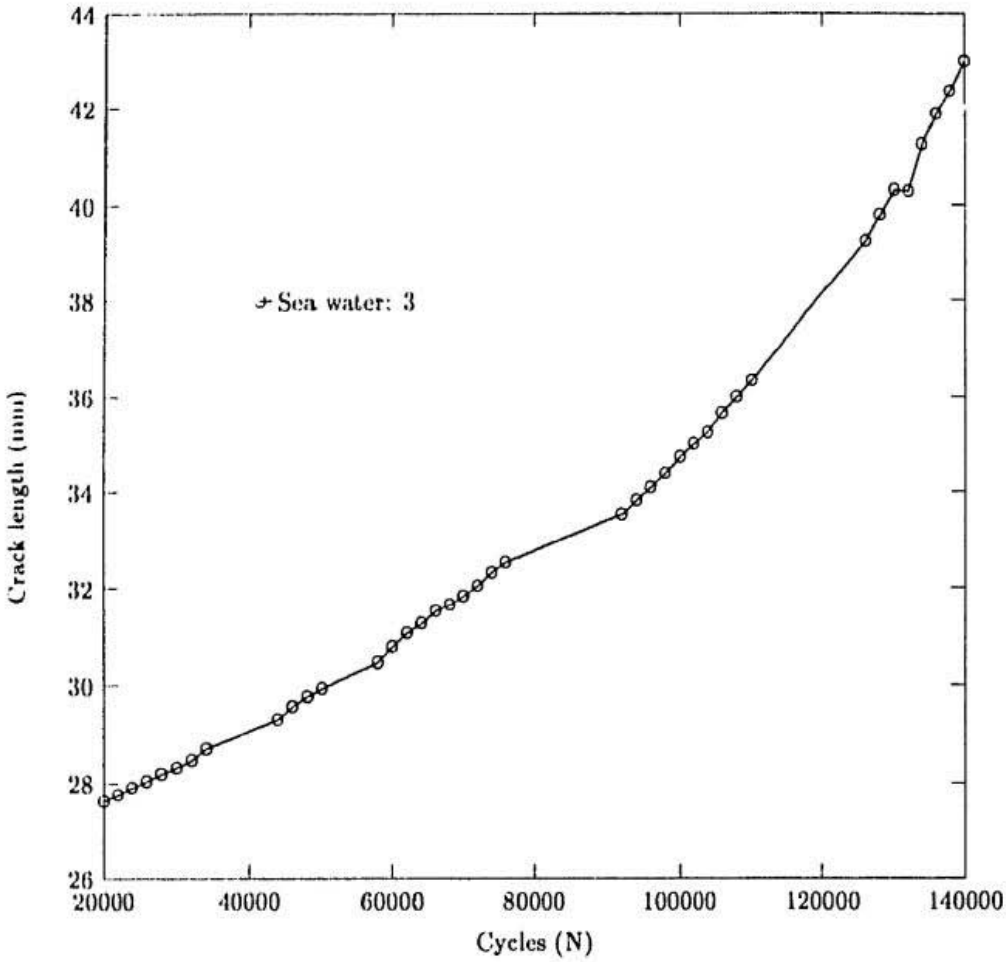

Figure 4.7: Crack growth curve for: sea water 3.

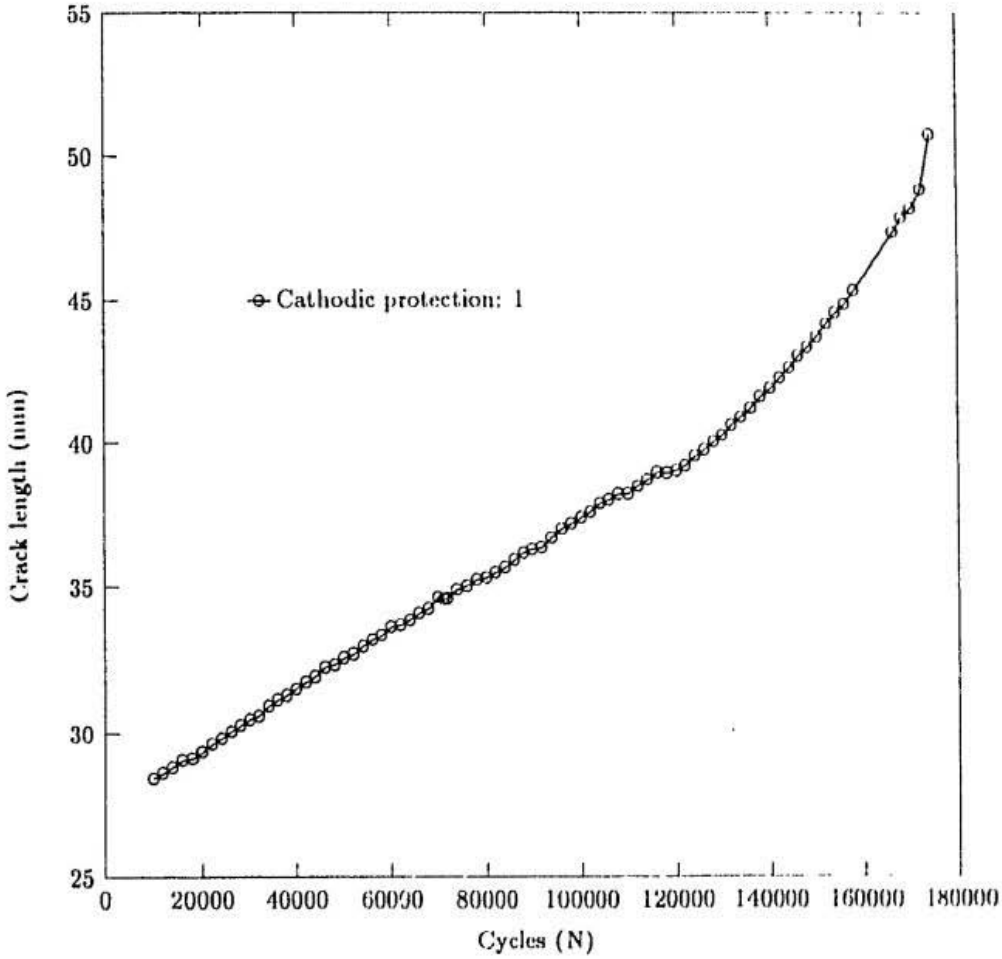

Figure 4.8: Crack growth curve for: cathodic protection 1.

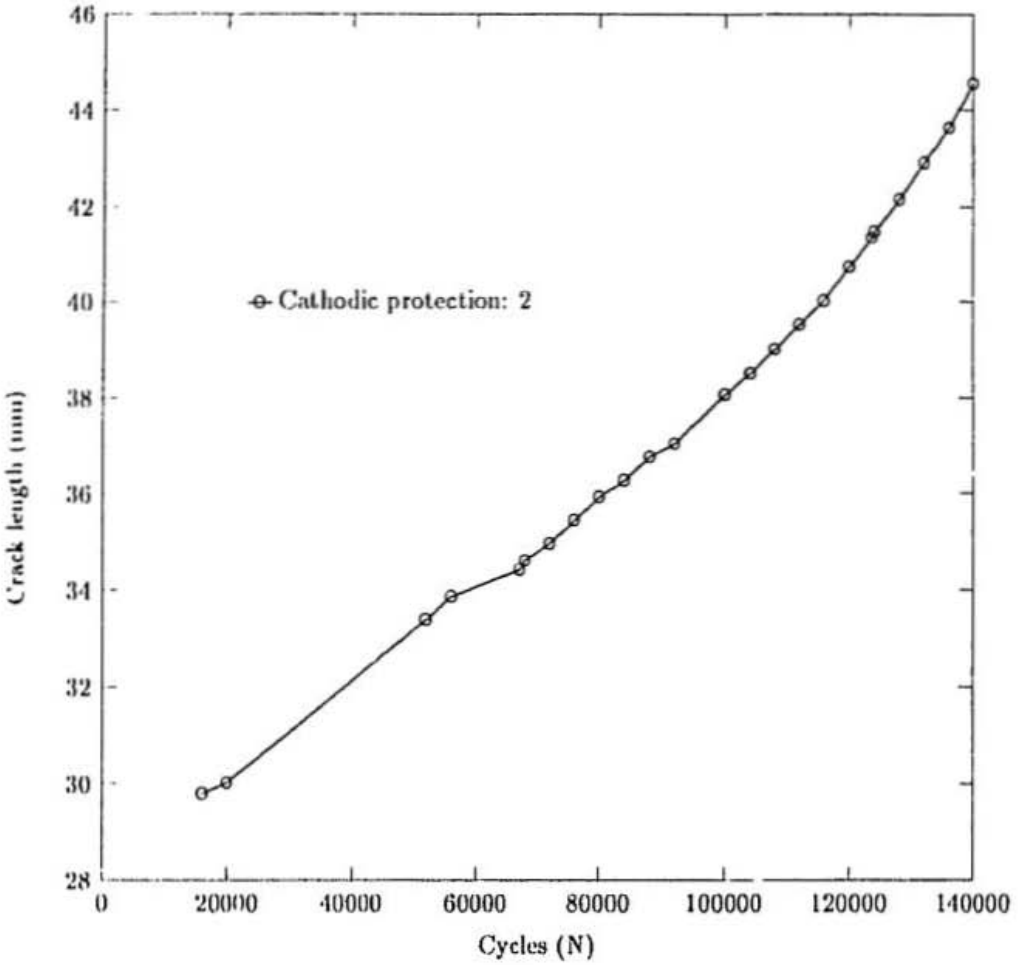

Figure 4.9: Crack growth curve for: cathodic protection 2.

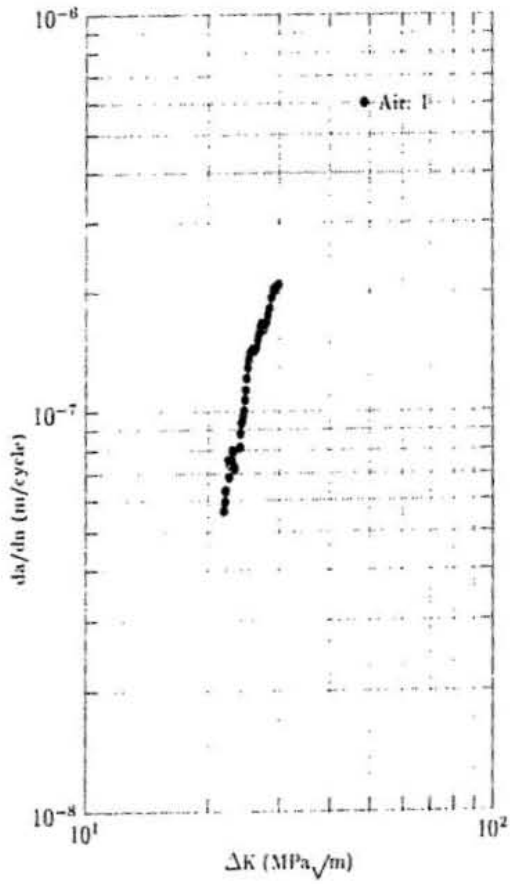

Figure 4.10: Air test: specimen 1.

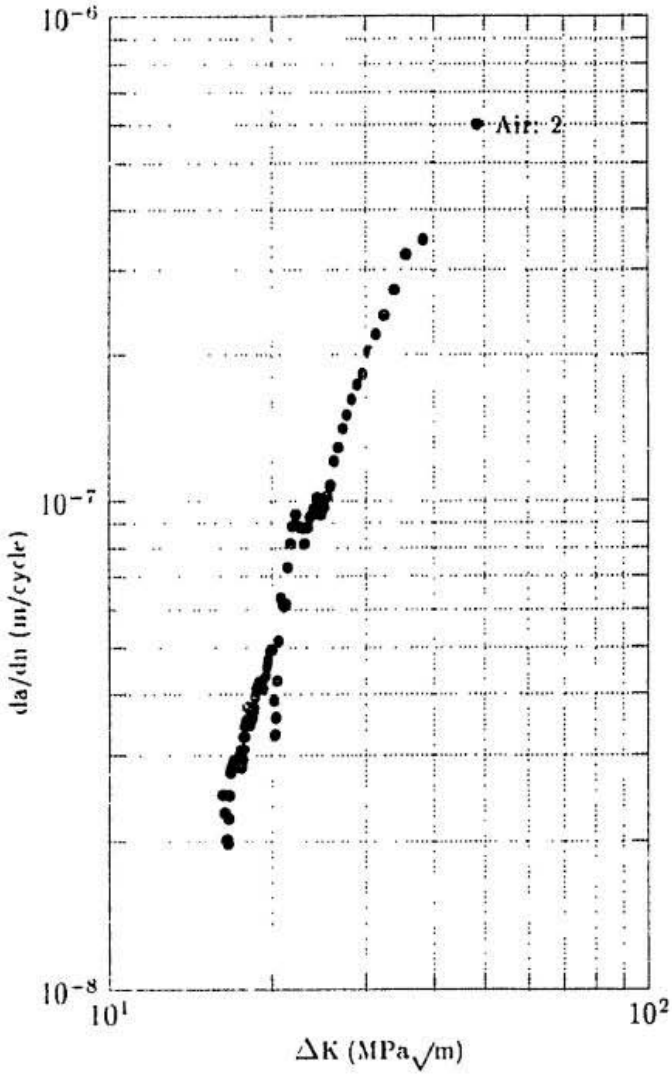

Figure 4.11: Air test: specimen 2.

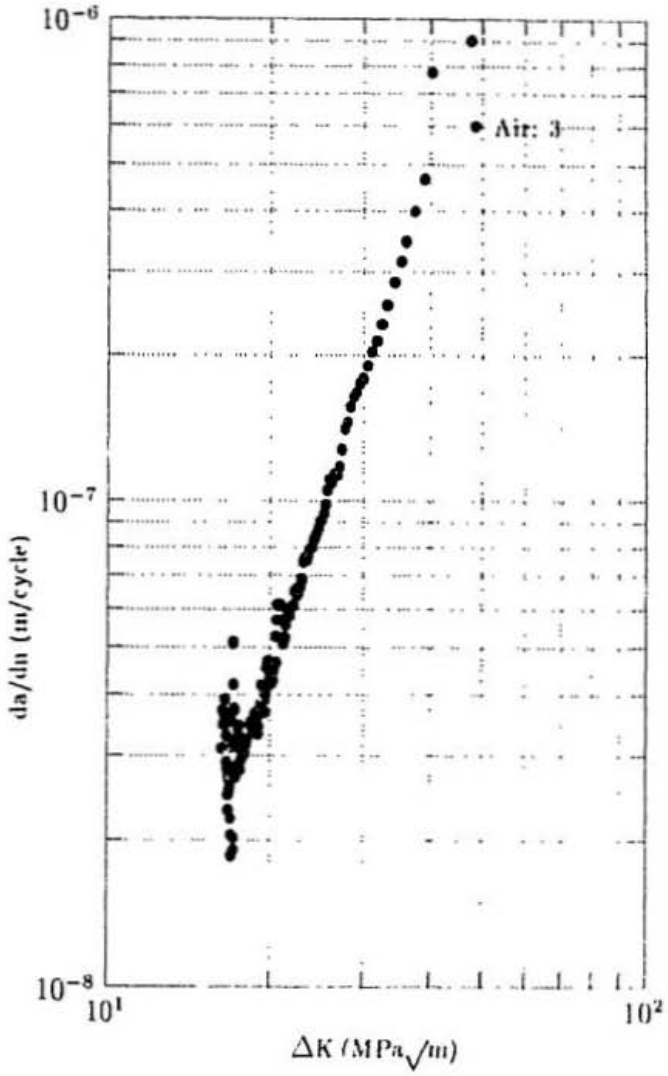

Figure 4.12: Air test: specimen 3.

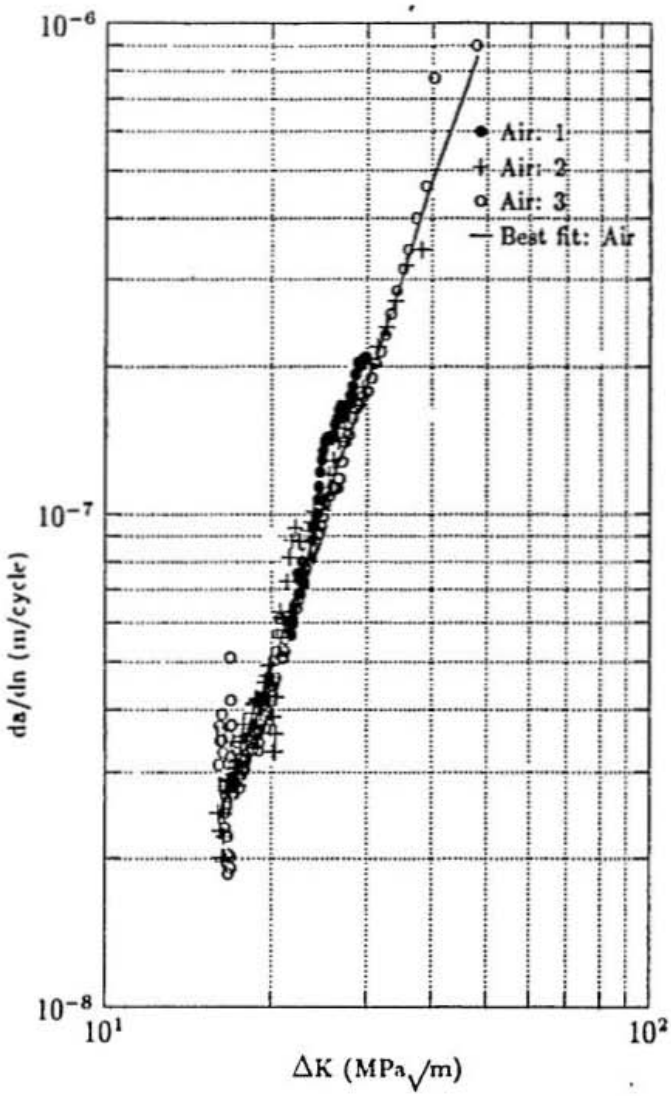

Figure 4.13: Air test: Best fit line.

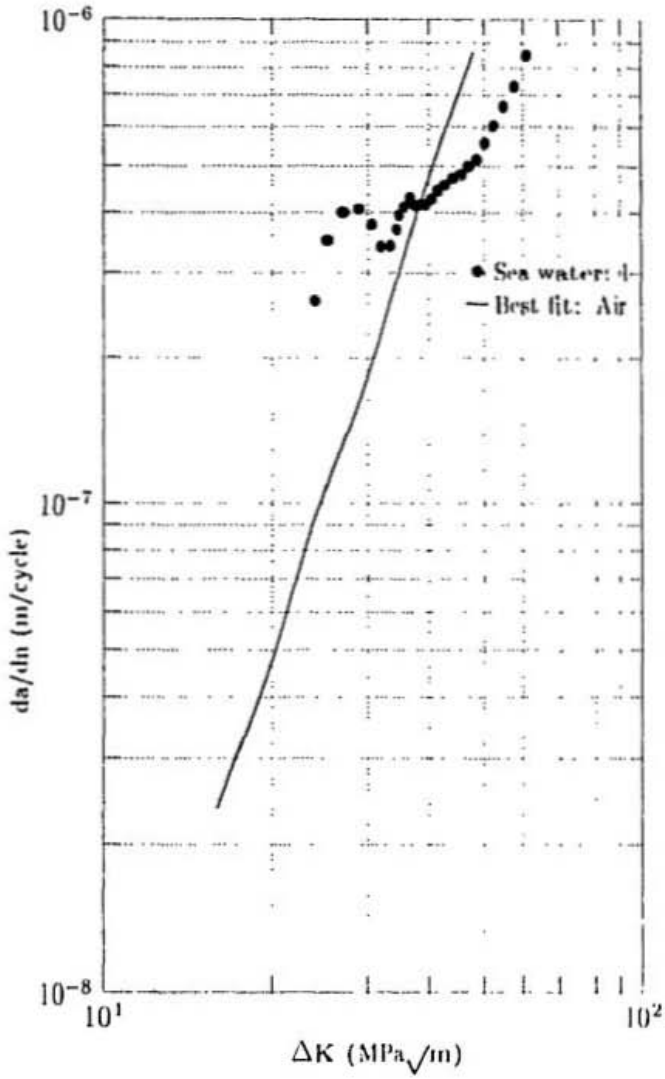

Figure 4.14: Sea water free corrosion: specimen 1.

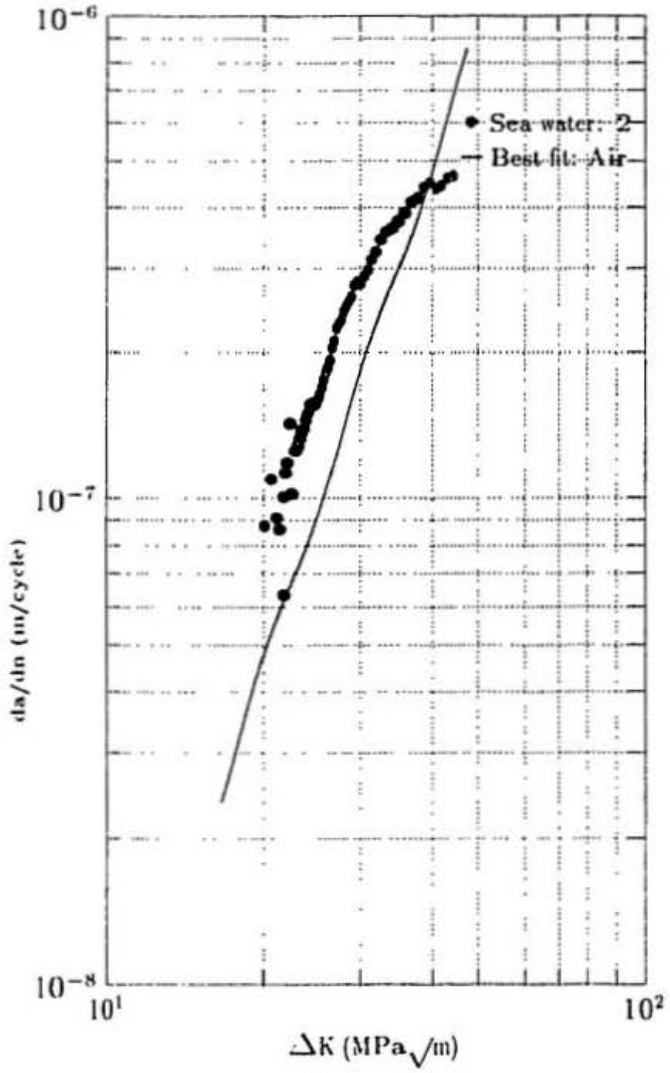

Figure 4.15: Sea water free corrosion: specimen 2.

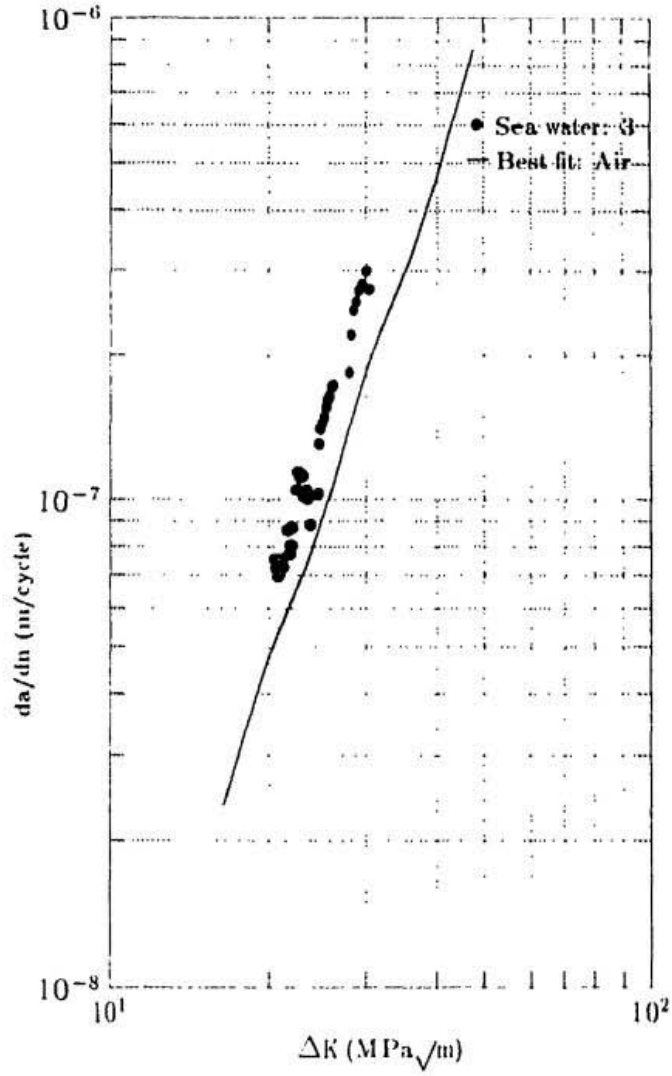

Figure 4.16: Sea water free corrosion: specimen 3.

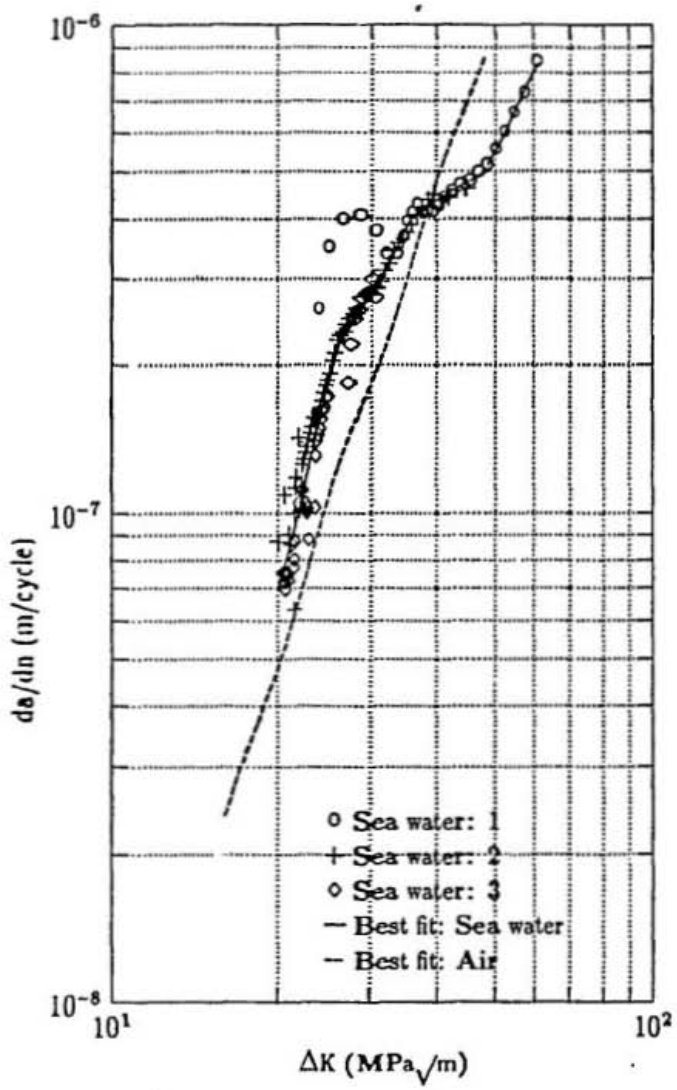

Figure 4.17: Seawater test: Best fit lines.

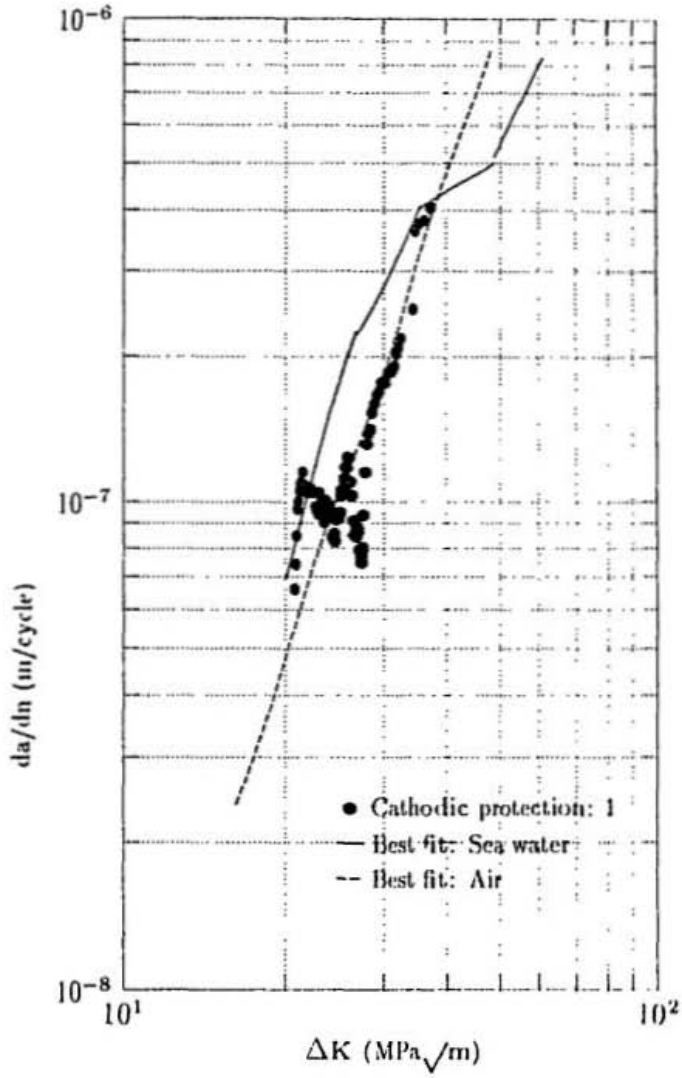

Figure 4.18: Cathodically protected: specimen 1.

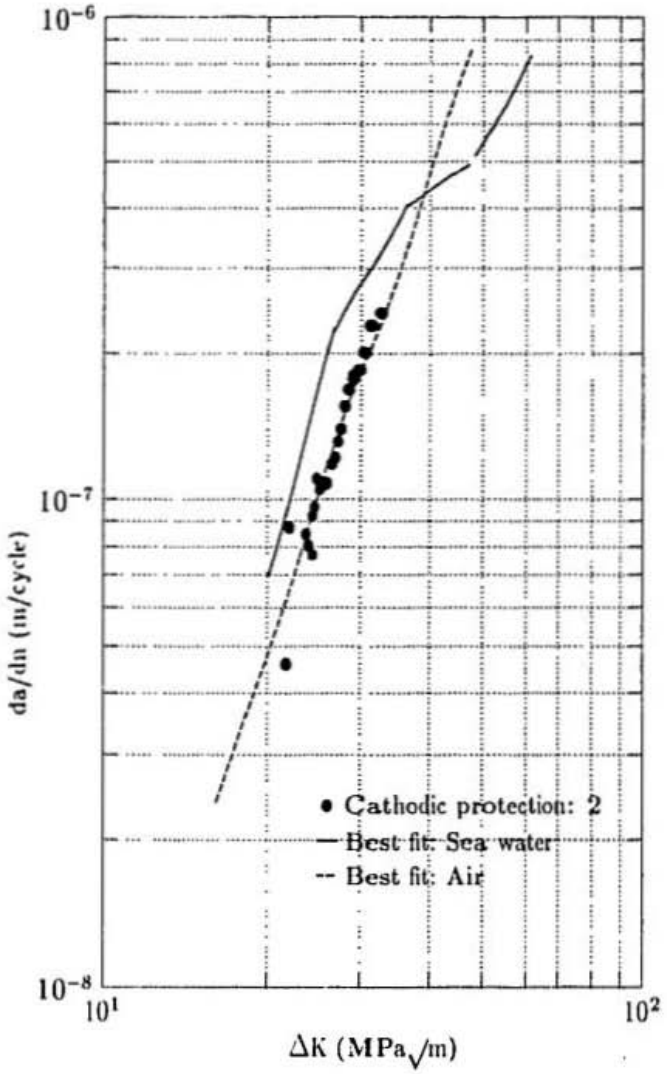

Figure 4.19: Cathodically protected: specimen 2.

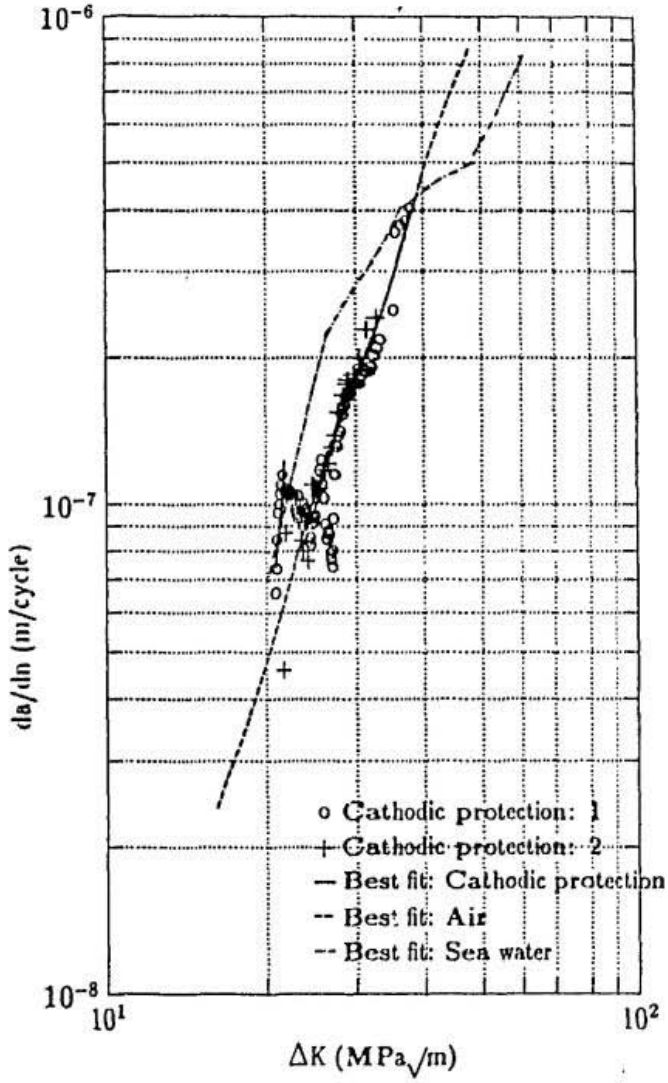

Figure 4.20: Cathodic protection test: Best fit lines.

4.5 Discussion of the results

The results from the experiments are presented in diagrams where the crack growth rate da/dN are plotted as a function of the stress intensity factor ΔK. The fatigue crack growth rate in air was selected as a base for comparing the behaviour of the base metal in other environments. The results for the tests conducted in air are grouped together and presented in figure 4.13. The data points are fairly well represented by the best fit straight line,

$$\frac{da}{dN} = 2.264 \times 10^{-12}(\Delta K)^{3.32} \qquad (4.5)$$

where, da/dN is in m/cycle and ΔK is in $MPa\sqrt{m}$.

The agreement between the three test results are fairly good with a little scatter at lower ΔK region. The threshold value ΔK_{th} in air is around 15-16$MPa\sqrt{m}$.

The influence of seawater was investigated and the results compared with the air test results are presented in figure 4.17. All the tests were conducted at a load ratio of 0.05 and at a frequency of 0.167Hz. The pH of the seawater was kept at 8.2. Very little change in pH occurred during the course of the experiment. The temperature of the seawater was kept constant at 5°C.

As can be seen from figure 4.17, the effect of seawater on the fatigue crack growth rate is not uniform over the range of ΔK . At smaller crack depths (lower ΔK) the crack growth rate is lower than in air. However, between a

ΔK value of 20 to 40MPa$\sqrt{m}$ crack growth exceed the air level. At a higher level of ΔK the influence of seawater was negligible. This is mainly because of the dominance of high ΔK over any chemical activity. Similar observations have been reported by Scholte and Wildscut (1981) and Austen, et. al (1981).

The effect of cathodic protection to the base metal was investigated by protecting the specimen with a cathodic potential of -830mV (SCE). The results obtained are presented in figures 4.18 and 4.19. As seen in figures 4.18 and 4.19 the crack growth rate is almost identical to the air values. At low ΔK (below 20MPa$\sqrt{m}$), the rate is below the air values. For a slightly higher ΔK (between 20-25MPa$\sqrt{m}$) there is a brief rise of the rate before it falls back to the air level. This sudden rise and fall of the crack growth rate was observed in both the specimens tested. It can be seen as a small plateau formation.

The plot for the specimen 1 (figure 4.18) shows a sudden drop in the crack growth rate value around ΔK of 25MPa$\sqrt{m}$ before it comes back to the air level very quickly. This abrupt departure from the steady state value coincides with a loading system failure and stoppage of the experiment for six to seven hours. There might have been a very small load keeping the crack face open while the anodic dissolution blunted the crack tip. As soon as the experiment started the crack tip regained its sharpness and crack growth rate value increased to the steady state level. From the results obtained from the cathodic protection tests, it can be concluded that a cathodic potential of

-830mV (SCE) eliminates any effect of sea water on the fatigue crack growth of the base metal.

Tests have also been conducted in seawater added with micro-bial nutrients. The results are reported in Appendix A.

Chapter 5

CONCLUSION

High strength offshore structural steel CSA G 40.21 M 350 WT was tested for corrosion fatigue performance in air, seawater, seawater with a cathodic protection of -830mV (SCE). Testing the metal in multiple media gave a chance to evaluate their relative severity.

The previous chapter thoroughly analyzed the results obtained from all the tests. In light of the above analysis the following conclusions can be drawn,

1. Free corrosion fatigue crack growth was about 1.5 to 2.0 times higher than in air. However, from ΔK values of 35MPa$\sqrt{m}$ upwards the crack growth rate declined below the air values. The ΔK_{th} value observed was more than that in air.

2. A cathodic protection potential of -830 mV (SCE) did not have much effect on ΔK_{th} . But, over rest of the ΔK range the crack growth rate was reduced to the level observed in air.

3. All the corrosion fatigue tests showed a higher ΔK_{th} than that in air.

5.1 Recommendation for further work

As discussed in the literature survey, micro-organisms like sulphate reducing bacteria play an important part in corrosion fatigue. As a next step from the present study, the effect of bacteria should be investigated. To support the bacteria life, nutrient chemicals have to be added to the standard ASTM seawater solution. It has been observed by Cowling and Hancock (1985) and also the present study (Appendix A) that the nutrients alone can alter the outcome of the tests. Tests have to be conducted in bacteria free, nutrient rich environment. Results from these tests can be compared with the results from the tests involving bacteria to obtain the net micro-bial corrosion fatigue. In view of the above discussion the following recommendations are made.

- Corrosion fatigue tests should be conducted with live sulphate reducing bacteria and the results should be compared with the sterile nutrient rich seawater tests.
- Efforts should be made to conduct bacteria tests without adding nutrient to the ASTM seawater solution. This would yield more realistic results and more accurately show the effect of bacteria.

References

1. ASTM, E647-78T, (1981), "Tentative Test Method for: Constant Amplitude Fatigue Crack Growth Rates Above 10^{-8} m/cycle," *Fatigue Crack Growth Measurement And Data Analysis*, ASTM STP 738, 1981, ed. Hudak, S. J., Bucci, R. J., ASTM, PA 19103, USA.

2. Assefpour-Dezfuly, M. and Fergusen, W. G., (1988), "Effect of Low Concentrations of Hydrogen Sulfide in Sea Water on Fatigue Crack Growth in a C Mn Structural Steel, *Corrosion Science*, Vol. 44, No. 7, July 1988. National Association of Corrosion Engineers.

3. ASTM, Designation: D1141-75, (March, 1990), "Standard Specification for Substitute Ocean Water," Annual Book of ASTM Standards.

4. Austen, I. M., Rudd, W. J. and Walker, E. F., (1981), "Factors Affecting Corrosion Fatigue and Stress Corrosion Crack Growth in Offshore Steel," paper no. 5.4, *International Conference, Steel in Marine Structures*, 5-8 Oct., 1981. Conference organised by the Commission of European Communities.

5. Brown, Floyd B., (1983), "Effects of Cathodic Protection on Corrosion Fatigue," *Corrosion Fatigue: Mechanics, Metallurgy, Electrochemistry and Engineering*, T. W. Crooker and B. N. Leis, Eds., American Society for Testing of Materials, 1983, pp. 508-515.

6. Cottis, R. A. and Moore, D. C. A., (1984), "Hydrogen Uptake by Steel Under Marine Fouling Growths," *Proceedings of 9th International Congress on Metallic Corrosion*, Toronto, 1984

7. Cowling M. J., Hancock J. W., (1985), "Fatigue Crack Growth in a Biologically Active Environment Under Realistic Load Sequences," *Draft Final Report, June, 1985*, Department of Mechanical Engineering, Glasgow University, Glasgow, G12 8QQ.

8. Daumas, S., Massiani, Y. and Crousier, J., (1988), "Microbiological Battery Induced by Sulphate-Reducing Bacteria," *Corrosion Science*, Vol. 28, No. 11, pp. 1041-1050, 1988.

9. Fuji, C. T. and Smith, J. A., (1983), "Environmental Influences on the Aquous Fatigue Crack Growth Rates of HY-130 Steel," *Corrosion Fatigue: Mechanics, Metallurgy, Electrochemistry and Engineering*, T. W. Crooker and B. N. Leis, Eds., American Society for Testing of Materials, 1983, pp. 390-402.

10. Harty, B. D. and Noël, R. E. J., (1990), "Corrosion Fatigue Cracking of Chromium Containing Steels," *Environmentally Assisted Cracking:*

Science and Engineering, ASTM STP 1049, ed. W. B. Lisagor, T. W. Crooker and B. N. Leis, American Society of Testing of Materials, Philadelphia, 1990, pp. 505-520.

11. Hamilton, Allan W., (1983), "The Sulphate Reducing Bacteria: Their Physiology and Consequent Ecology," *Microbial Corrosion, Proceedings of the conference sponsored and organized jointly by The National Physical Laboratory and Metals Society and held at NPL Teddington on 8-10 March 1983*, The Metals Society, London, 1983, pp. 1-5.

12. Iverson, W. P., (1966), *Science*, Vol. 151, pp. 986, 1966.

13. Iverson, W. P. and Olson, G. J., (1983), "Anaerobic Corrosion by Sulfate-reducing Bacteria Due to Highly Reactive Volatile Phosphorous Compound," *Microbial Corrosion*, The Metals Society, London, 1983.

14. Jones, W. J. D. and Blackie, A. P., (1990), "Cyclic Tension Corrosion Fatigue of High-Strength Steels in Sewawater," *Environmentally Assisted Cracking: Science and Engineering, ASTM STP 1049*, W. B. Lisagor, T. W. Crooker and B. N. Leis, Eds., American Society for Testing and Materials, Philadelphia, 1990, pp-447-462.

15. Kawashima, Asahi, Hashimoto, Koji and Shimodaria, Saburo, (1976), "Hydrogen Electrode Reaction and Hydrogen Embrittlement of Mild

Steel in Hydrogen Sulfide Solutions," *Corrosion-NACE,* Vol. 32, No. 8, August, 1976.

16. King R. A. and Miller, J.D.A., (1971), "Corrosion by the Sulphate-reducing Bacteria," *Nature,* vol. 233, pp. 491-492.

17. Maahn E., (1981), "The Influence of Cathodic Protection on Crack Growth Rate in Fatigue of Steel in Water," paper no. 5.3, *International Conference, Steel in Marine Structures,* 5-8 Oct., 1981. Conference organised by the Commission of European Communities.

18. Morgan, H. G., Rance, A., Sylvester, D. R. V. and Scott, P. M., (1981), "An Investigation of the Corrosion Fatigue Crack Growth Behaviour of Structural Steels in Seawater," paper no. 5.1, *International Conference, Steel in Marine Structures,* 5-8 Oct., 1981. Conference organised by the Commission of European Communities.

19. Ouchi[1], H., Kobayashi, J. and Soya, I., (1990), "The Effects of Stress Waveform and Frequency on Fatigue Crack Growth Rates in a Steel Immersed in Sea Water," *Environment Assisted Fatigue, EG F7,* ed. P. Scott, Mechanical Engineering Publications, London, 1990, pp. 17-30.

20. Ouchi[2], H., Soya, I., Ebara, R. and Yamada, Y., (1990), "Effects of Temperature and Dissolved Oxygen in Seawater on the Fatigue Strength of Welded Steel Joints," *Environment Assisted Fatigue, EG*

F7, ed. P. Scott, Mechanical Engineering Publications, London, 1990, pp. 17-30.

21. Panasyuk, V. V. and Romaniv, O. N., (1980), "The Mechanics of Corrosion Fatigue of Metals and Alloys," *Corrosion Fatigue*, ed. Parkins, R. N. and Kolotyrkin, Ya. M., *Proceedings of the First USSR-UK Seminar on Corrosion Fatigue of Metals*, Lvov, USSR, 19-22 May, 1980, The Metals Society and Freund Publishing House Ltd., London, pp. 24-35.

22. Paris, P. and Erdogan, F., (1963), "A Critical Analysis of Crack Propagation Laws," *Journal of Basic Engineering*, December, 1963, ASME, pp. 528-534.

23. Postgate, John Raymond, (1979), *The Sulphate Reducing Bacteria*, Cambridge University Press, Cambridge, GB.

24. Rajpathak, S. S. and Hartt, W. H., (1988), "Fatigue Crack Initiation of Selected High Strength Steels in Sea Water," Proc., Offshore Mechanics and Arctic Engineering Conference, 1988, Vol. III, pp. 323-331.

25. Rhee, H. Chong and Delgado, Jorge H., (1992), "Fracture and Corrosion Fatigue Crack Growth Properties of High Strength Riser Coupling Material," Proc., Offshore Mechanics and Arctic Engineering Conference, 1992, Vol. III-B, pp. 533-547.

26. Salvarezza, R. C. and Videla, H. A., (1980), "Passivity Breakdown of Mild Steel in Sea Water in the Presence of Sulphate Reducing Bacteria," *Corrosion- NACE*, Vol. 36, No. 10, October, 1980, pp. 550-554.

27. Scholte, H. G., Wildschut, H., (1981), "Fatigue Crack Propagation Tests on Welded Specimens in Air and Sea Water," paper no. 5.2, *International Conference, Steel in Marine Structures*, 5-8 Oct., 1981. Conference organised by the Commission of European Communities.

28. Tubby, Peter J. and Booth, Geoffrey S., (1992), "Corrosion Fatigue Crack Growth Rate Studies in Two Weldable High Strength Steels," Proc., Offshore Mechanics and Arctic Engineering Conference, 1992, Vol. III-B, pp. 539-547.

29. Turnbull, A. and Carroll, M. W., (1990), "The Effect of Temprerature and H_2S Concentration on Hydrogen Diffusion and Trapping in a 13% Chromium Martensitic Stainless Steel in Acidified NaCl," *Corrosion Science*, Vol. 30, No. 6/7, pp. 667-679, 1990.

30. Venugopal, V. and Putatunda, S. K., (1990), "Influence of Overload and Temperature on Stress Corrosion Crack Growth Behaviour in a Low-Alloy Steel," *Environmentally Assisted Cracking: Science and Engineering, ASTM STP 1049*, W. B. Lisagor, T. W. Crooker and B. N. Leis, Eds., American Society for Testing and Materials, Philadelphia, 1990, pp. 42-58.

31. Von Wolzogen Kuhr, C. A. H. and Van der Vlugt, L. S., (1934), *Water*, Vol. 18, pp. 147.

Bibliography

1. Arup,Hans, Maahn.E., Jacobsen,F. and Press.Palle, (1986), "Environmental Effects in Corrosion Fatigue," ECSC Agreement no. 7210 KG. 901, Final Report.

2. Barsom, J. M. and McNicol, R. C., (1974), "Effect of Stress Concentration on Fatigue Crack Initiation in HY-130 Steel," ASTM STP 559, American Society for Testing and Materials, Philadelphia. 1974.

3. Briant, C. L., (1985), *Metallurgical Aspects of Environmental Failures.Material Science Monographs; 12,* Elsevier Science Publishing Company Inc., 52, vanderbuilt Ave., NY, USA.

4. Hartt, William, (1981), "Fatigue of Welded Structural Steel in Sea Water," *13th Annual Offshore Technology Conference*, Huston, Texas. 1981. OTC 3962.

5. Hamilton, Allan W., (1987), "Sulphate-reducing Bacteria and the Mechanism of Corrosion in the Marine Environment," *Microbes in the Sea*, ed. M. A. Sleigh, Ellis Harwood Limited, Chichester, GB, 1987, pp.

190-202.

6. Hi Jgins, Charles M., Casad, Burton M., Schroeder R. L. and Patton, Charles C., (1970), "The Effect of Cathodic Protection on the Corrosion Fatigue Behaviour of Carbon Steel in Synthetic Sea water," *2nd Offshore Technology Conference*, Huston, Texas, 1970, OTC 1254, pp. II257-II264.

7. Jelinek, J. and Neufeld, P., (1982), "Kinetics of Hydrogen Formation From Mild Steel in Water Under Anaerobic Conditions," *Corrosion-NACE*, Vol. 38, No. 2, February, 1982, pp. 98-104.

8. King, R. A., Miller, D. A. and Smith, J. S., (1973), *British Corrosion Journal*, vol. 8, pp. 137, 1973.

9. Marine Industry Advisory Services, MIT Sea Grant Program, (1984), "Marine Corrosion and Bio-fouling, Opportunity Brief #37," *Report #MIT SG-84-5, Grant no. NA81AA-D-00069, Project no. A/M-2*, MIT, Cambridge, Massachusetts 02139.

10. Novak, S. R., (1983), "Corrosion Fatigue Crack Initiation Behavior of Four Structural Steels," *Corrosion Fatigue: Mechanics, Metallurgy, Electrochemistry and Engineering, ASTM STP 801*, T. W. Crooker and B. N. Leis, Eds., American Society for Testing and Materials, 1983, pp. 26-63.

11. Ogundale, G. I. and White, W. E., (1986), "Some Observations on the Corrosion of Carbon Steel in Sour Gas Environments; Effects of H_2S and $H_2S/CO_2/CH_4/C_3H_8$ Mixtures," *Corrosion- NACE*, Vol. 42, No. 7, July, 1986, pp.398-408.

12. Stranger-Johannessen, Maria, (1983), "Offshore Structures at Risk from Sulphate Reducing Bacteria," *Offshore Engineer*, February, 1983, pp. 51.

13. Tiller A. K., (1983), "Electrochemical Aspects of Microbial Corrosion: an Overview," *Microbial Corrosion, Proceedings of the conference sponsored and organized jointly by The National Physical Laboratory and The Metals Society and held at NPL Teddington on 8-10 March 1983*. The Metals Society, London, 1983, pp. 54-65.

14. Walch, Marianne and Mitchell, Ralph, (1983), "The Role of Microorganisms in Hydrogen Embrittlement of Metals," *Paper no. 249, Corrosion '83, The International Corrosion Forum Sponsored by the National Association of Corrosion Engineers*, Anheim Convention Center, Anheim, California, April 18-22, 1983, pp. 249/1 - 249/8.

Appendix A

Some work on the live tests (involving bacteria) has been done. This includes designing the set up and testing in nutrient rich seawater. So far at least one test attempted using bacteria. The results are declared invalid because of a lack of sufficient growth of bacteria population and sulphide production. It has, in all probability, to do with a faulty bacteria culture rather than the experimental set up itself. In fact, the set up was found to be highly capable of sustaining bacteria life (ie., 1. capable of supplying an oxygen free atmosphere, 2. maintaining a steady temperature and 3. providing an extremely limited but steady circulation of base solution without sweeping away any bacteria).

Live test set up

Because of the special requirements of the live tests a completely new set up (from the sterile corrosion fatigue tests) was adapted. The test chamber (figure A.1) was made air tight and the space above the water surface is

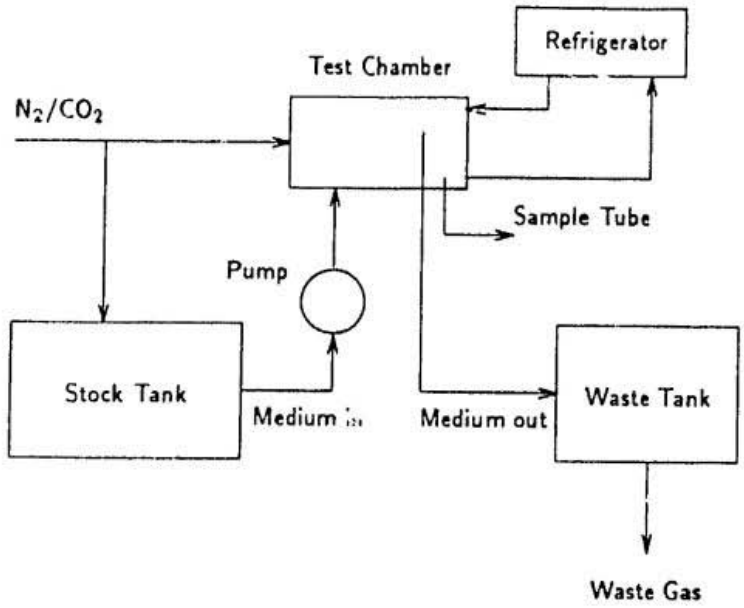

Figure A.1: Live test setup

constantly supplied with an inert gas mixture of N_2 and CO_2. The pressure of the gas mixture was kept slightly above the atmospheric pressure to make sure that air does not leak into the system. Like the sterile tests, base solution is circulated from a stock tank. The flow rate was kept very low to avoid sweeping out any bacteria. The free space of the stock tank was also supplied with the inert gas mixture. A flexible rubber tubing formed a joint between the top loading pin and the top cover of the main test chamber. This insured air tightness and free vertical movement of the loading system.

Nutrient tests

The tests in nutrient rich seawater were done in the standard (sterile) corrosion fatigue test set up. However, the circulation of sewater was eliminated. This was done to closely model the live tests. The purpose of testing in this environment was to find the absolute effect of the presence of bacteria, since the added nutrients alone can produce different results than standard seawater.

Prepartion of base solution

First the standard ASTM seawater ws prepared and the nutrients were added to it. The constituency of the chemicals (table A.1)was such that the final solution closely resembles the Postgate-B medium (Postgate 1979). The pH of the seawater alone was around 8.1. When the nutrients were added the pH came down to 4.98. Specimen 1 was tested in pH 4.98. However, for specimen two (figure A.3) pH was adjusted up to 5.9.

Yeast extract	1g
Ascorbic acid	0.1g
KH_2PO_4	0.5g
NH_4Cl	1g
$FeSO_4.7H_2O$	0.004g
Thioglycollic acid	0.4g
Sodium lactate	14g

Table A.1: Nutrients in per liter of ASTM seawater

Nutrient test results

The tests involving seawater with added nutrients were conducted in two different pH levels. Test 2, (pH 4.98) showed (figure A.3) a plateau below ΔK of 30. Test 1 (figure A.2) with pH of 5.9 did not show any particular plateau. However, both showed slopes less than either the air or seawater tests (figure A.4). Crack growth rate was about 1.5-2 times higher than under free corrosion. Beyond a ΔK of 40, both the tests produced a crack growth rate close to that in air.

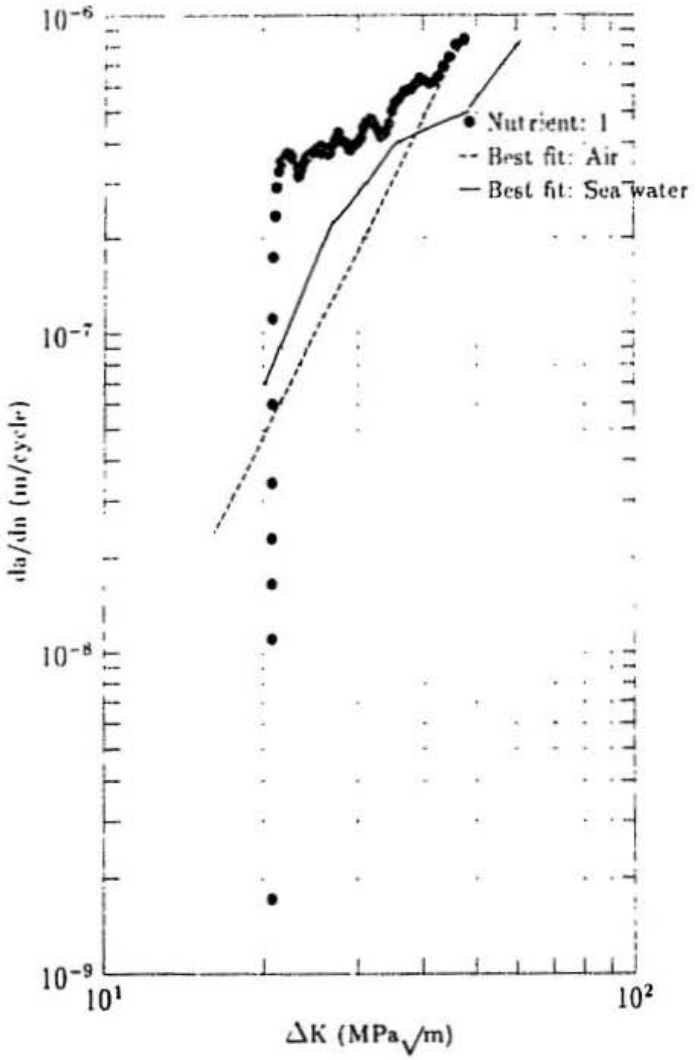

Figure A.2: Neutrient test: specimen one

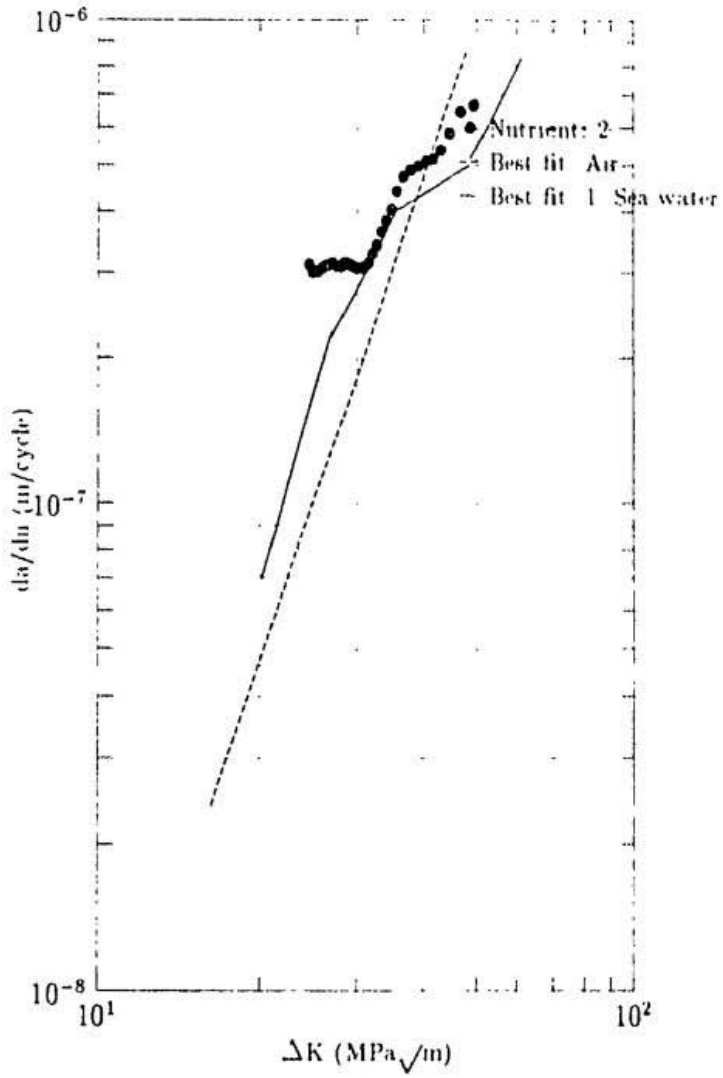

Figure A.3: Nutrient test: specimen two

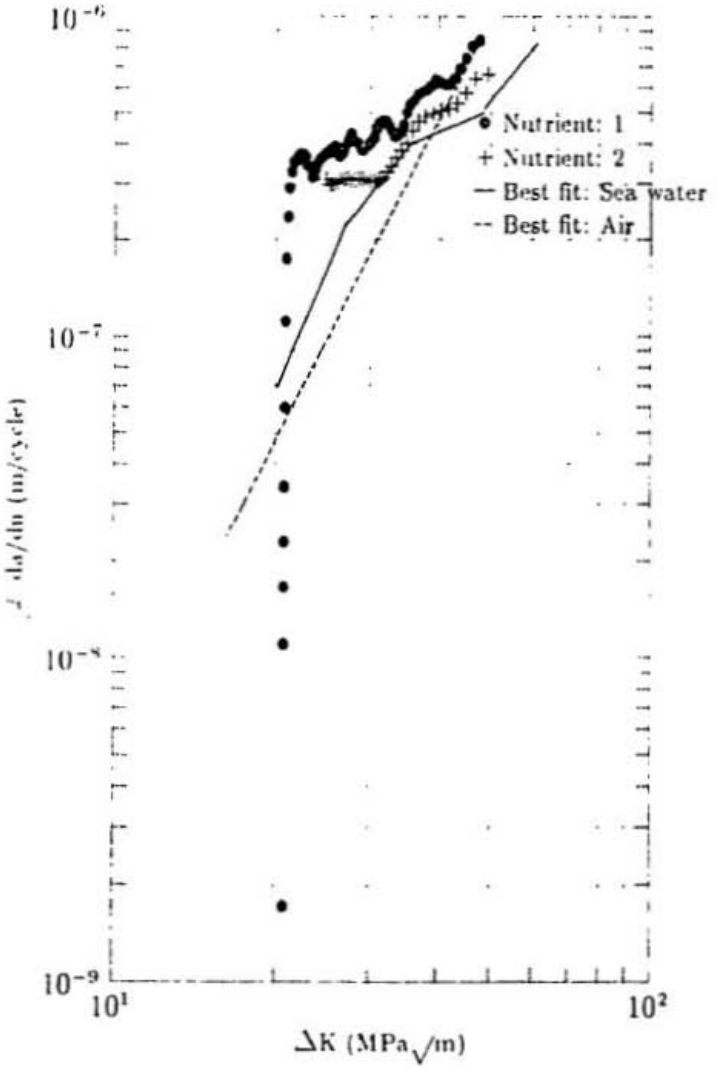

Figure A.4: Nutrient test: specimen one and two